The effect of organic matter degradation on the rheological behaviour of natural mud

J.T.P. de Klerk

The effect of organic matter degradation on the rheological behaviour of natural mud

by

J.T.P. de Klerk

to obtain the degree of Master of Science
at the Delft University of Technology,
to be defended publicly on Tuesday January 19, 2022 at 14:00.

Student number:	4388674
Project duration:	March 8, 2021 – January 19, 2022
Thesis committee:	Dr. ir. S. Miedema, TU Delft, chairman
	Dr. C. Chassagne, TU Delft, supervisor
	Dr. ir. J. Gebert, TU Delft
	Ir. A. Shakeel, TU Delft

An electronic version of this thesis is available at http://repository.tudelft.nl/.

TUDelft

Abstract

The nautical bottom is defined as the level where physical characteristics of the bottom reach a critical limit beyond which contact with a ship's keel causes either damage or unacceptable effects on the controllability and manoeuvrability of ships. The nautical bottom is usually assessed using the density of the bottom fluid mud layer as a criterion. However, for navigability purposes, rheological properties of bottom layers (and in particular yield stress), rather than density, are key parameters. The rheological properties of fluid mud depend on both the density and composition of mud and this composition can vary over time, owing to organic matter degradation.

In this study, the influence of organic matter degradation on the rheological properties of mud is investigated. A total of 129 samples from different locations and mud layers (depths) from the Port of Hamburg were analysed. They were degraded in the laboratory under aerobic and anaerobic conditions for 250 days. The rheological properties of these samples were analysed before and after degradation using a rotational rheometer (HAAKE MARS I).

The rheological properties of the samples before and after anaerobic degradation were significantly dissimilar. On average, the fluidic yield stress decreased by 26 %. This percentage had a strong positive correlation with the total organic carbon contents and degradabilities of the samples under consideration. In contrast, the seasonal variability of the samples did not show any correlation with the rheological properties.

After degradation, the decrease in total organic carbon content is small and could not be correlated to yield stress changes. This leads to conclude that the structural breakdown of organic matter and/or the breakdown of organic bridges between organic matter and clay particles are the reasons for the decrease in strength.

The fluidic yield stresses of the aerobically degraded samples increased by 2 %. The difference with their anaerobically degraded counterparts is suspected to be caused by oxidation, which could add cohesion to the mud. From this study, it can be concluded that intentional organic matter degradation during dredging operations could be very effective in making the mud navigable.

Acknowledgements

Contents

1

Introduction

1.1. Context

In order to load or unload cargo, commercial vessels require navigable waterways to move within a port. Since these ports are naturally built near the shoreline, sediment deposition is a problem (McAnally et al., 2007a, Pellegrini et al., 2020). Some areas may naturally be deep enough, but sedimentation will ultimately lead to an unacceptable loss of water depth in most places. As port authorities should ensure safe navigation for all designated waterways, it is their responsibility to manage the sediment properly (Kirichek et al., 2018).

1.1.1. Sedimentation

The characteristics of this sediment vary for every location, as they depend on the discharge from the rivers and seas carrying it in (Leys and Mulligan, 2011). Waterborne sediment can be a valuable resource, as it can form rich farmland. Though despite its value, too much sediment can also cause environmental and economic problems (Sharp et al., 2010). Sediment management is therefore crucial for ports, as its entrainment and accumulation can limit human activity (Pellegrini et al., 2020). The most used technique to counteract this limitation is regular maintenance dredging (Bianchini et al., 2019).

1.1.2. Dredging

In 2015 over one hundred and forty million cubic meters of sediment were dredged in Europe alone. Germany was the most significant contributor, followed by Belgium and the Netherlands (OSPAR, 2016). Germany's largest port, the Hamburg Port Authority, annually contracts several million cubic meters of maintenance dredging, originating from the Elbe river (Gebert et al., 2019). Though dredging is a proven method for sediment removal, it comes with several drawbacks like the temporary prohibition of navigation (Pellegrini et al., 2020). Furthermore, dredging has a significant impact on the environment, as it disrupts the macrobenthic community and has a large carbon footprint (Rehitha et al., 2017).

1.2. Sediment management systems

Over the years, engineers have found multiple techniques to help manage port sedimentation. These methods can be divided into three categories; (1) methods that keep sediment out, (2) methods that remove deposited sediment and (3) methods that keep sediment moving (McAnally et al., 2007b, Sharp et al., 2010).

Methods that keep sediment out can be effective when the entrance to the port lies 'on' a tidal river. With these Entrance Flow Optimalisation Systems (EFOS), a flow-deflecting wall in the river is installed (figure 1.1). This wall deflects a part of the river that flows into the port entrance. A sill is then installed on the bottom of this small channel, shielding the port from the denser near-bed suspensions (Kirby, 2010). An EFOS installed at Kölnfleet, Hamburg, has shown a 45 % reduction in siltation rate (Parker and Kirby, 1982).

Nevertheless, while 45 % is impressive for a passive device with no moving parts or fuel consumption, it is unlikely that these devices will reduce the total sediment rate in a big port like Hamburg or Rotterdam. Most methods used in these ports fall into the second category; removing deposited sediment. The most commonly used management system is called the passive nautical bottom approach (McAnally et al., 2007b).
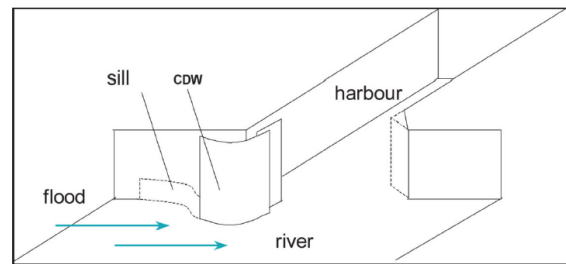
Figure 1.1: A schematic depiction of a EFOS, taken from Kirby, 2010

1.2.1. Passive nautical bottom approach

In this approach, the decision of whether sediment does or does not yet need to be removed is determined using the nautical bottom. The definition of the nautical bottom is often only dependent on the density of the mud; from a specific density, the mud is not navigable anymore. The Permanent International Commission for Navigation Congresses (PIANC) defined the nautical bottom approach as: "The level where physical characteristics of the bottom reach a critical limit beyond which contact with a ship's keel causes either damage or unacceptable effects on controllability and manoeuvrability" (PIANC, 2014) . Most ports currently use the density for this "physical characteristic", determining a threshold for the nautical depth, as depicted in figure 1.2.
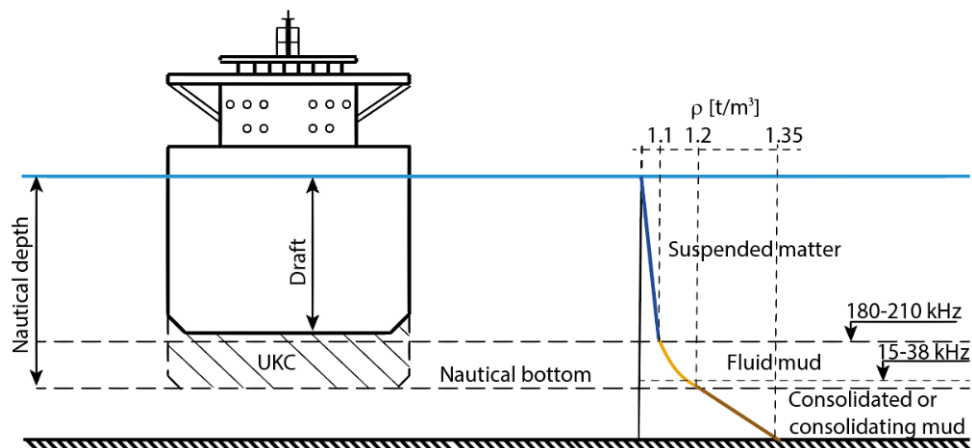
Figure 1.2: A schematic depiction of determining the nautical bottom. In this instance the nautical bottom is set at the density limit of 1200 [kg/m^3]. Taken from Kirichek et al., 2018.

As shown in table 1.1 this passive definition for the nautical bottom is adopted in various ports in Europe and Asia. By measuring, the depth from which the mud in an area of the port has become unnavigable according to the port's threshold can be checked. Traditionally this is done using acoustic signals, though this technique has limitations. A fluid mud layer is hard to detect acoustically because of its weak density gradient (Kirby et al., 2015). However, more precise techniques have been proposed; one of the most accurate alternative methods is based on scattered and transmitted gamma-radiation. While this and other techniques can determine the density of the water column, they can often only do so in one dimension. Therefore these techniques are often combined with the traditional acoustic signals to form a spatial map (Kirichek et al., 2018).

Once (a part of) the port is on the verge of becoming unnavigable, the port authorities will still need to dredge the area to ensure safe passage to vessels. Therefore, the Passive Nautical Bottom approach does not solve the sediment issue entirely.

Port	Density [tonnes/m^3]
Rotterdam	1,2
Bangkok	1,2
Paramaribo	1,23
Zeebrugge	1,151-1,347
Yangtze	1,25
Liang Yungang	1,25-1,30
Yianjing Xingang	1,2-1,3
Avonmouth	1,2
Dunkirk	1,2
Bordeaux	1,2
Nantes-Saint Nazaire	1,2

Table 1.1: Density criteria for navigable depth, taken from McAnally et al., 2007b

1.2.2. The active nautical bottom approach and in-situ conditioning

A sediment management system that does solve the problem without the need for maintenance dredging is called the active nautical bottom approach. In this approach, the mud is agitated by a hopper dredger, fluidized inside a conditioning vessel and returned to a near-Newtonian condition (McAnally et al., 2007b, Kirby, 2010). When placed back onto the bed, this causes the mud to flow back into the water column. It is also possible to bring the mud into a state where settling rates are prolonged for up to several months. This is called in-situ conditioning and can make the mud keep its fluidity and navigability (Kirby, 2010).

The latter technique has been used successfully in the port of Emden since 1990 (and later in the port of Bremerhaven) (Kirby, 2010). In the port of Emden, the mud is kept aerobic through treatment in a conditioning vessel. By keeping the mud in an oxygenated condition on the conditioning vessel, exopolymeric substances can continuously be produced by aerobic bacteria once back on the bed (Kirby, 2010). These substances ensure the mud preserves its fluidity by trapping the interstitial water. The dredging costs have been reduced from 12,5 to 4 million euros/year in the port of Emden (Kirby, 2010), making it a success. However, Bremerhaven and Emden's ports are relatively small and do therefore not form any proof that in-situ conditioning could work in a bigger port like Rotterdam or Hamburg. For big ports, the passive nautical bottom approach is still the standard.

1.2.3. Shortcomings

The yield stress is the leading property determining whether or not a ship can sail through fluid mud. Density is relatively easy to measure in situ, and therefore easy to use in a threshold. However, it is commonly accepted that density is not the only parameter influencing yield stress. A recent study into fluid mud from the port of Hamburg comparing natural with diluted samples confirmed this (Shakeel et al., 2020d). From the results of this study, shown in figure 1.3, a dissimilarity in yield stress is visible from two samples with the same density. One of the main reasons for this inconsistency is the lack of organic matter in the diluted samples. Furthermore, the particle size distributions of these locations were similar throughout the harbour. The differences in yield stresses from different locations from the port of Hamburg can therefore not be attributed to particle sizes variations.

The dependency of the yield stresses on the total organic carbon (TOC) content was recently shown by comparing several locations from the port of Hamburg with different TOC contents (Shakeel et al., 2020c). These results can be seen in figure E.1. These TOC contents differ from season to season. This is another reason why the density threshold for the whole year is inaccurate. As technology evolves and new measurement techniques become available, improved management systems will not only be density-based.

1.2.4. Alternatives

Evidently, density does not have a conclusive relation with the safety of sailing through natural mud. Therefore, new definitions for the nautical bottom are suggested to be based on the rheology of the
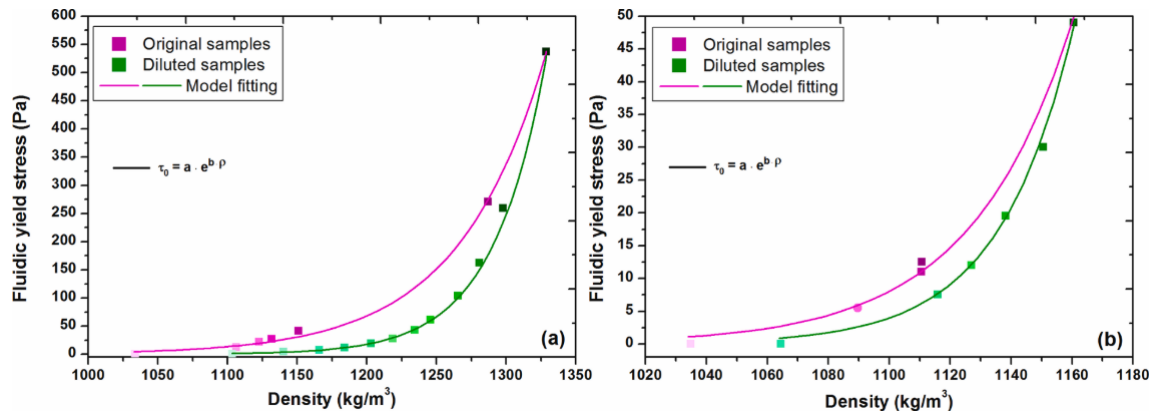
Figure 1.3: Fluidic yield stress values as a fuction of density for natural and diluted samples from two locations (a and b). The solid lines represent a model fitting. Taken from Shakeel et al., 2020d

mud (McAnally et al., 2007b). Though the results of the port of Emden do not guarantee successes elsewhere, they have shown rheology-based techniques can be effective. By using these new nautical bottom approaches, the efficiency of the procedures could be increased significantly, reducing costs and greenhouse emissions. However, to use these new nautical bottom approaches, further research on the rheological properties of natural mud is needed.

1.3. Problem statement

The organic matter content in natural mud changes over time due to degradation (McAnally et al., 2007a; Zander et al., 2020). The structure caused by this organic carbon is assumed to give strength to natural mud. This is due to polymer chains and the interaction with clay particles of these chains (forming flocs). Moreover, these flocs can even further interact with each other forming a network of flocs (Shakeel, MacIver, et al., 2021). This will be elaborated further in section 2.1.

The literature shows that fluid mud from the port of Hamburg will also degrade (Zander et al., 2020). In this process, the organic carbon will partly be released as carbon dioxide and methane (Gebert et al., 2019). Assuming the organic matter (OM) indeed causes increased 'strength' to the samples, the degradation of this matter could thus affect the rheological properties.

A clear understanding of these rheological properties is needed to develop new sediment management techniques. However, no research has been done into the effect of OM degradation on these properties, while this cannot be overlooked. This research aims to fill this knowledge gap.

1.4. Research objective

Clearing the path to improved sediment management techniques by quantifying one unknown variable; the effect of organic matter degradation on the rheology of mud.

1.5. Research questions

In order to achieve this objective, the main research question is formulated; what are the effects of organic matter degradation on the rheological properties of natural mud?

In order to find the threshold of navigable mud, the yield stresses of different layers of mud must be predicted. It has been proven that the presence of OM is one of the factors influencing the rheological properties (Shakeel et al., 2020c). This suggests its degradation may also affect the rheological properties of natural mud. In order to solve the main research question, it is divided into several sub-questions;

- 1. Does the effect of organic matter degradation on the rheology of mud differ for different densities?

In this research, several vertical mud layers are considered. From top to bottom, these are called: fluid mud (FM), fluid mud to pre-consolidated (FM/PS), pre-consolidated sediments (PS), pre-consolidated to consolidated sediments (PS/CS), and consolidated sediments (CS)(Shakeel, Kirichek, et al., 2019).

The density of these layers increases with depth. Furthermore, the organic turnover decreases with density (Zander et al., 2020). This suggests that the strength of mud samples with a relatively low density will be affected more than samples with high densities. Leading to the hypothesis: the rheological properties of a denser layer of mud are less affected by OM degradation than those of a less dense layer. Several samples from the same location but different mud layers will be examined.

- 2. What is the effect of different amounts of organic matter on the rheology of mud before and after degradation?
Suppose degradation turns out to influence the rheology (lower shear stress and viscosity). In that case, it stands to reason that a bigger OM content would result in a bigger decrease in yield stress and viscosity. Therefore the following hypothesis will be tested: the rheology of mud with a relatively large amount of OM will be affected more by degradation than the rheology of mud with a relatively small amount of OM. This will be tested by comparing degraded samples from different locations, as the amount of OM of these locations differs.

- 3. What is the effect of the degradability of the present organic matter on the rheology of natural mud?
A sample containing OM with a higher degradability will lead to a more significant % of the present OM getting degraded (Zander et al., 2020, Gebert et al., 2019). As it is the OM that causes additional strength within the mud (Shakeel et al., 2020c), a mud layer with faster degrading OM is expected to become weaker than an otherwise identical sample containing slower degrading OM. Therefore, the following hypothesis will be tested: The rheological properties of an (otherwise similar) mud layer with a higher degradability are more affected than a sample with a lower degradability. This will be tested by comparing samples with different degradabilities.

- 4. Is there any seasonal variability on the effect of organic matter degradation on the rheology of mud?
Some environmental conditions like temperature and light vary due to seasonal changes and may influence the OM quantities or turnover. Directly because chemical processes may go faster/slower, or indirectly through their influence on the presence of microorganisms (some OM is consumed by microorganisms, as explained in section 2.2.1(Zander et al., 2020)). Therefore, they may influence the effect of degradation on the rheological properties. Therefore the following hypothesis will be tested: The effect of OM degradation on the rheological properties of mud is not affected by seasonal changes. The samples under investigation were taken on different campaigns in different seasons. The hypothesis will be tested by comparing (otherwise identical) samples from different campaigns.

- 5. Does the effect of organic matter degradation on the rheology of mud differ for aerobic and anaerobic conditions?
The different mud layers (FM, FM/PS, PS, PS/CS and CS) behave differently over time; the denser layers are more stable and, concurrently, have a relatively low oxygen supply. Furthermore, the liquid mud may move around more due to factors as tides and ships passing by. This movement causes a relatively high oxygen supply. Aerobic or anaerobic degradation of OM leads to different chemical reactions with different products (Zander et al., 2020). These different products could cause different effects on the rheological properties of the mud. F. Zander found the carbon release under aerobic conditions of around three to five times higher than anaerobic conditions (Zander et al., 2020). This leads to the hypothesis: aerobic degradation has a more significant impact on the rheological properties of mud than anaerobic degradation. This will be tested by comparing (otherwise identical) samples which are degraded in aerobic and anaerobic conditions.

1.6. Approach

To answer these questions, natural mud samples were taken from several locations of the port of Hamburg. They have been obtained from different depths, locations and campaigns. Furthermore, these samples have been degraded under different circumstances (aerobic/anaerobic) by F. Zander, who analysed the degradation of OM (Zander et al., 2020). Afterwards, these samples, which have thus

been degraded in controlled environments, were used in this research. The 'fresh' samples were also tested by A. Shakeel, and the results were used as a comparison for the degraded samples.

2

Literature

A summary of some of the literature relevant to this study is provided in this chapter. In the first section, some basic rheological principles will be presented. Subsequently, the degradation of organic matter will be introduced, and to what extent this happens in the port of Hamburg.

2.1. Rheology

Rheology is the study of the flow and deformation of matter. When a continuum is subjected to external forces, only three equations are needed to describe all relations; the equation of motion, the continuity equation and the constitutive equation. In order to use these, however, first, all properties of a material need to be defined. These properties can be measured by experiments designed to produce the kinematics present in the definition of the rheological property (i.e., material function). When the needed stress components are then measured, the required rheological property can be determined (Morrison and Morrison, 2001). The science behind this activity is called rheometry.

2.1.1. Rheological measurements

Instruments designed to test rheological properties are called rheometers. They can be divided into two types; extensional- and shear-rheometers. One example of an extensional rheometer is a melt flow indexer. In a melt flow indexer, a load is applied on the material whilst the cylinder (or barrel in figure 2.1) is heating the material. This combination causes the material to flow through the die at a certain speed. After 10 minutes, the Melt Flow Index is defined as the weight of the material extruded with a certain pressure, temperature and die diameter applied (Shenoy and Saini, n.d.).
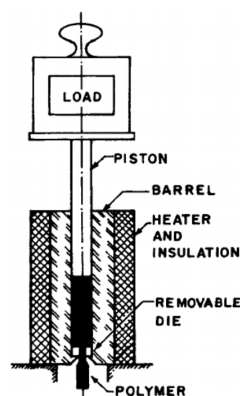
Figure 2.1: A Schematic diagram of a melt flow indexer. Taken from Shenoy and Saini, n.d.

Rotational rheometers
One type of shear rheometer is the rotational rheometer, which will be used in this research (figure 2.2). Two types of rotational rheometers exist; controlled shear rate and controlled shear stress. With a controlled shear rate rheometer, a specific shear rate is applied to the sample, and the device measures the stress it needs to produce to deliver this shear rate. A controlled shear stress rheometer works the opposite (i.e. delivers shear stress and measures shear rate). However, with a feedback loop programmed within the rheometer, modern rheometers can be set to perform experiments both ways.

Figure 2.2: Rotational rheometer HAAKE MARS I

2.1.2. Introduction to rheology
If a liquid follows Newton's law of viscosity (Newtonian fluids) it is considered a normal liquid. However, if a fluid follows neither Newton's law of viscosity nor Hooke's law of elasticity, it is considered a complex fluid (Morrison and Morrison, 2001).

Newtonian fluids
Most liquids with low molecular weight are Newtonian fluids. Water, alcohol and benzine all belong to this group, for example. Also, all gases and most solutions of simple molecules are Newtonian fluids. Newtonian fluids obey the Newtonian constitutive equation 2.1 (Morrison and Morrison, 2001). A constitutive equation is, by definition, not a fundamental law of nature but rather a quantitative relation between two parameters. The parameters are physical quantities (in this case, the shear stress τ and shear rate $\frac{dv_i}{dx_k}$), and the relationship is specific for every material (here the viscosity μ). The viscosity is thus constant and independent of the shear rate for a Newtonian fluid.

$$\tau_{ki} = -\mu \frac{dv_i}{dx_k} \tag{2.1}$$

Complex fluids
From a rheological perspective, complex fluids are more interesting. For these fluids, the viscosity changes with one or more external conditions (Morrison and Morrison, 2001). Complex fluids can show complex rheological behaviours like (Pūtaiao, 2010);

- Shear-thinning; the viscosity decreases with increased stress (tomato sauce)

- Shear thickening or dilatant; the viscosity increases with increased stress (cornstarch)

- Rheopectic; the viscosity increases with stress over time (cream)

- Thixotropic; the viscosity decreases with stress over time (honey)

- Bingham yield stress; the fluid resists flowing until the Bingham yield stress is reached (peanut butter)

For a fluid to be considered complex, it should not follow Hooke's law of elasticity (Morrison and Morrison, 2001). Fluid mud, however, is a viscoelastic fluid, meaning it does show solid-like behaviours (Shakeel, Kirichek, et al., 2019). Furthermore, yield stresses have also been observed in numerous experiments. Some of the most important rheological phenomena observed in fluid mud will now be explained, followed by descriptions of experiments with which these phenomena can be shown and measured.

2.1.3. The rheology of fluid mud

Fluid mud can have many sources, each with its own solids content. This makes the generalisation of the flow properties complex (McAnally et al., 2007a). Furthermore, these properties are heavily dependent on the solids content. The rheological properties of mud are assumed to be related to the network structure within the mud (McAnally et al., 2007a, Kirichek et al., 2018). The structures consist of mud flocs, with long polymer chains (i.e. organic matter) keeping the flocs in place. These structures influence rheological phenomena and properties present in the fluid (Shakeel et al., 2020a). By defining and quantifying these properties, the differences between samples can be compared. The most important properties will be quickly touched upon in the next section.

Viscoelasticity

If liquid mud is subjected to stress, it deforms, like all fluids. When this stress is removed, Newtonian fluids (like water or oil) are at rest directly after. In viscoelastic fluids like mud, however, the stress inside does not instantaneously vanish (Morrison and Morrison, 2001). The structures within the mud described earlier give it these solid-like properties.
If a material is subjected to a strain in the form of $\gamma(t) = \gamma_0 sin(\omega t)$, the shear stress response can be written in the form of equation 2.2 (McAnally et al., 2007a).

$$\tau(t) = \tau_0 \sin(\omega t + \delta) = \gamma_0 \left(G' \sin \omega t + G'' \cos \omega t \right) \tag{2.2}$$

This equation relates the amplitudes of the strain γ_0 and stress τ_0, phase difference δ, frequency ω and time t with the moduli G' and G''. The storage modulus G' represents the Hookean modulus of elasticity, and the loss modulus represents the viscous part (Nie et al., 2020). If G'' equals zero, the response is purely elastic. If G' equals zero, the material is purely viscous. The proportions of G' and G'' are thus shown by the phase angle δ. This relation will be used extensively in the tests, as described in chapter 3.

Yield stress definition

Yield stresses are important for a variety of applications and provide additional parameters for better characterisation for yield-stress materials (Ahuja et al., 2020). Therefore a clear definition must be specified. As defined by Shakeel et al., 2020e, the static yield stress τ_y^s and fluidic yield stress τ_y^f used in this research will be defined as depicted in figure 2.4. As shown, the trend above the yield stress and the trend below the yield stress are extrapolated. Then the yield stresses are defined as the stress at which these extrapolated lines cross.

Shear thinning with yield stresses

When little stress is applied to the mud, the structures within the mud are believed to cause the relatively high viscosity measured in experiments (Shakeel, Kirichek, et al., 2019). In this phase, the completely structured fluid mud can give the most elastic, solid-like responses. In figure 2.4 the results of a stress sweep are shown. In a stress sweep, the mud is subjected to increasing shear stress while measuring the resulting rotation. This way, the viscosity can be obtained. The first stage, in which the flocs of mud are still in a fully structured matrix, is depicted in the upper left corner of this graph.
When the applied stress is increased further, however, the structures will break. The stress at which this occurs is conventionally referred to as the static yield stress τ_y^s (Shakeel et al., 2020e). As the flocs lose the structure keeping them together, they can now move more freely. This causes the viscosity of the mud to decrease significantly (in the domain of 2 to 3 Pa in figure 2.4).

When the stress is increased even further, a new viscosity plateau is observed. Only recently, some insight has been gained on the reason for this halt in shear-thinning behaviour. Using a modified form of RheOptiCAD (Shakeel, van Kan, et al., 2019), the formation of cylindrical structures have been observed. Varga et al. observed this phenomenon in weakly attractive suspensions (Varga et al., 2019). He attributed this to a log-rolling mechanism between the shear-inducing surfaces, as he depicted in 2.3. These long and hollow flocs seem to be the reason the mud can resist the additional shear until the so-called fluidic yield stress τ_y^f is reached (Shakeel, MacIver, et al., 2021).
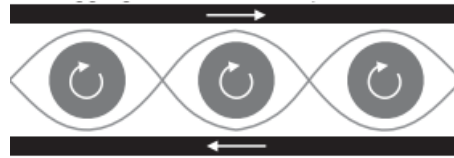
Figure 2.3: A schematic depiction of log-rolling between the shear-inducing surfaces. Taken from Varga et al., 2019.

At applied stresses from this point upward, the flocs themselves will start to fall apart. This causes the viscosity to drop even further, as all particles can now move around even more freely. A schematic image is shown with the corresponding stress range in the bottom right corner of figure 2.4.
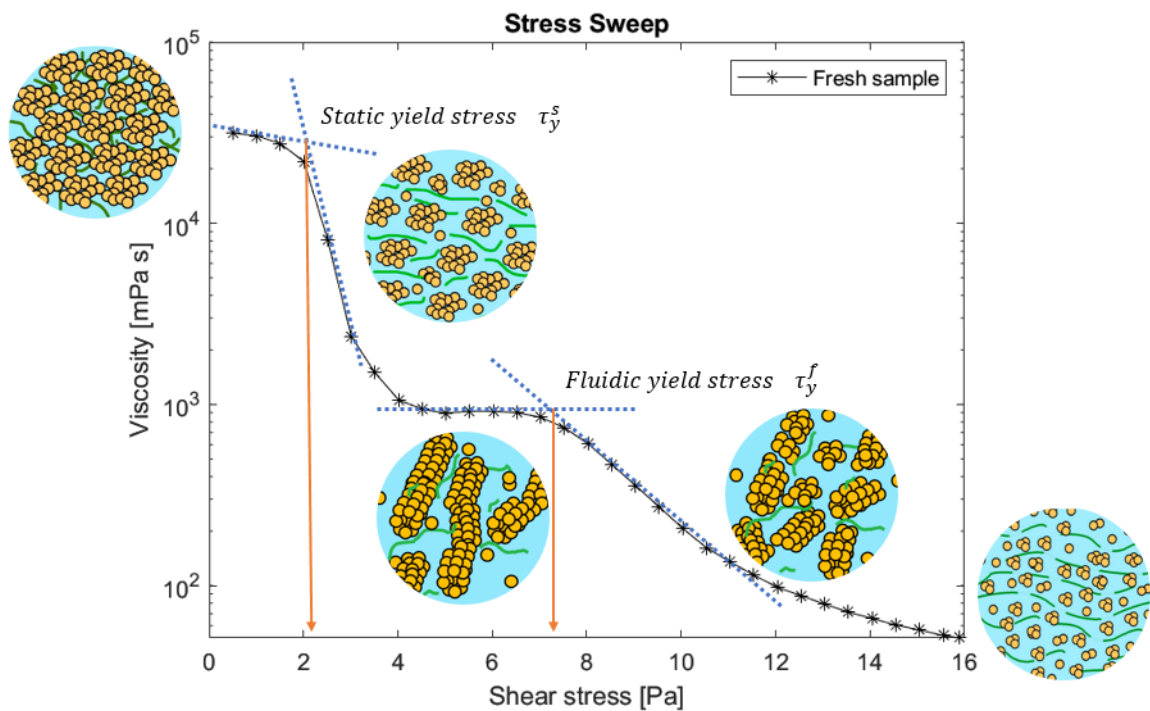
Figure 2.4: A schematic representation of the different stages of the stress sweep with their particle structures.

Furthermore, this figure clearly shows that as the stress increases, the viscosity decreases. Therefore this sample, which is the same fluid mud this research is interested in, is shear thinning.

Thixotropy

Once the structure of natural mud has been broken, the viscosity is thus at its lowest point. These structures can not rebuild themselves instantaneously. If the shear stress were to be lowered again, the viscosity would therefore not necessarily be similar to at the start of the experiment. After some time, however, the initial structure within the mud could return in a process named structural recovery. This ability is what gives natural mud its thixotropic characteristics.

Non-newtonian fluids are considered thixotropic if the viscosity decreases over time when constant

shear stress is applied. Subsequently, the viscosity recovers in time once this stress is removed (Shakeel et al., 2020b). In such conditions, fluid mud exhibits these characteristics (McAnally et al., 2007a) and is thus considered thixotropic.

One experiment designed to investigate thixotropic behaviour is called the thixotropic loop (or, hysteresis loop). An example is provided in figure 2.5. In this experiment, the shear rate is first gradually ramped up (upper line), then held constant for a period of time and then decreased back to zero again (lower line). When the sample is thixotropic (like the example), the shear rate ramp up increasing rate (i.e. structural breakdown) is higher than the decreasing rate of the shear rate ramp down (i.e. structural recovery) (Shakeel et al., 2020c). The clockwise loop formed in figure 2.5 is called the hysteresis loop, and if it is anti-clockwise, the behaviour observed is anti-thixotropy or negative thixotropy (Shakeel et al., 2020c).
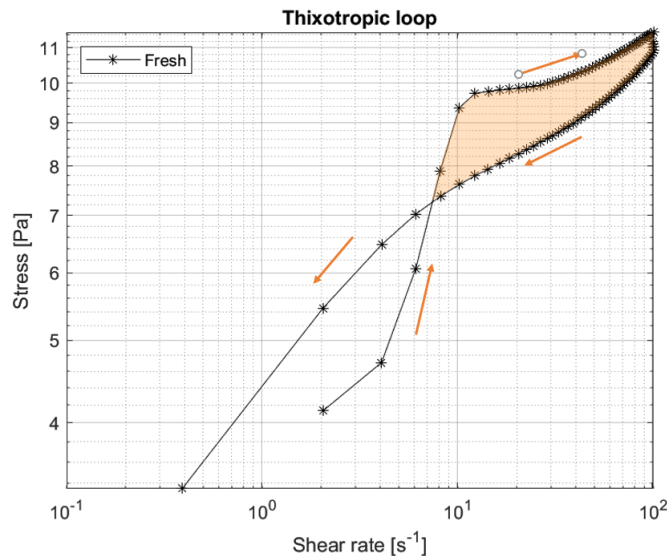
Figure 2.5: An example of a thixotropic loop experiment. The arrows indicate the chronological order of the acquired data. The orange surface represents the hysteresis loop.

The downside of studying the thixotropic properties with a thixotropic loop is the shear rate. Since the thixotropy is measured using viscosity, a shear rate needs to be applied constantly to measure the viscosity. However, the sample can never recover fully while the shear rate is applied.

Structural recovery

Studying rheological properties over a period of time without disturbing the sample is a challenge. Mewis et al. first came up with a method (Mewis and de Bleyser, 1972) which has been applied on many materials, including liquid natural mud (Shakeel et al., 2020b). In this method, the first step of testing the thixotropic properties is determining the storage modulus before shearing, G_0'. Then a sample is sheared destructively for a certain amount of time. Thereafter the mud is allowed time to recover. When the mud is fully recovered, the equilibrium storage modulus can be obtained, G_∞'. This experiment is discussed more thoroughly in chapter 3.

Using this structural recovery method, A. Shakeel (Shakeel et al., 2020b) found that for a relatively low destructive shear rates ($<35\,\text{sec}^{-1}$) G_∞' will be lower then the storage modulus before shearing, G_0'. But after a destructive shearing process with relatively high shear rates ($>35\,\text{sec}^{-1}$) G_∞' will be higher then G_0'. A. Shakeel gave a possible explanation for this behaviour, as shown in figure 2.6 (Shakeel et al., 2020c).

According to this possible explanation, a pre-shearing process with shear rates under 35 per second will only be partly destructive. The structure formed by the organic matter in the mud will break, but the flocs remain intact. As the organic matter forms new bonds with the flocs, the structural recovery
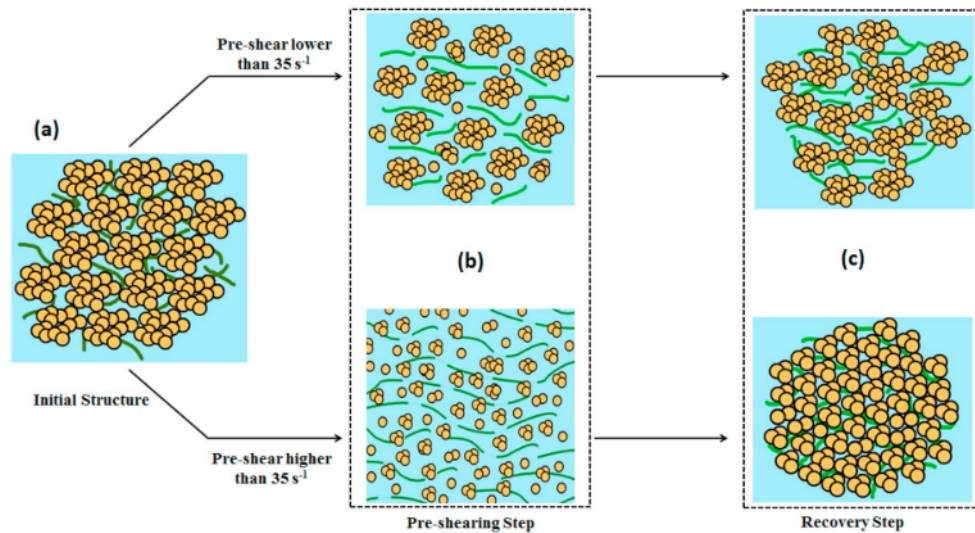
Figure 2.6: A schematic illustration of the structural breakup and recovery at different shear rates. Taken from Shakeel et al., 2020b.

will, in time, cause the mud to regain some of its strength. Nonetheless, the strength of the original structure can not be regained, resulting in $G'_\infty < G'_0$. Shear rates above 35 seconds will understandably be more destructive. After shearing, not only the structure provided by the organic matter but also the flocs themselves will have been disrupted. As the floc-sizes have been reduced, a densification of the network can now take place. After the structural recovery a matrix stronger then the initial structure will be formed, causing $G'_\infty > G'_0$.

2.2. Organic matter degradation

Sediment, sediment-bound organic matter and suspended organic matter flows into the port of Hamburg from two sides. Upstream the Elbe river transports the sediment from its catchment. These sediments contain a relatively more significant share of autochthonous and lighter organic matter, such as planktonic biomass. The sediments from the other source, the North sea, are transported by repeating land inward streams resulting from tidal pumping. These sediments contain heavier organic matter with a predominantly allochthonous origin, like plant litter and eroded soils. (Boehlich and Strotmann, 2008, Zander et al., 2020).

Organic matter (OM) has different sources. Natural sources include plant litter, phytoplankton and eroded terrestrial topsoils, whereas anthropogenic sources include urban sewage and surface runoff (Zander et al., 2020, Gebert et al., 2019). The OM from natural sources originates from photosynthetic activity, which can be represented by the simplified reaction 2.3 (De Leeuw and Largeau, 1993).

$$CO_2 + H_2O \overset{\text{light}}{\rightarrow} ''CH_2O'' + O_2 \tag{2.3}$$

Here, the different types of organic compounds produced by photosynthetic organisms (i.e. biopolymers) are represented as $''CH_2O''$. As explained in section 2.1, these compounds provide structure to the mud. However, this structure might not last indefinitely as OM is prone to degradation.

2.2.1. Degradation

The OM can be directly oxidised to CO_2, reduced to CH_4, or partly oxidised to intermediate compounds. The benthic process (i.e. not direct oxidation) proceeds via enzymatic reactions (Arndt et al., 2013). OM degradation thereby controls nutrients and inorganic carbon recycling, influencing the organic carbon flux to deeper terrestrial layers. Consequently, the net CO_2 flux from the atmosphere is partly determined by the OM degradation process (Arndt et al., 2013).

The susceptibility of light fraction OM to degradation is relatively high (Gebert et al., 2019). The planktonic biomass, for instance, degrades considerably faster than terrestrial biomass (Grasset et al., 2018). This difference can be attributed to different levels of resistance of the biopolymers or the pre-ageing, which some heavier fractions have already undergone (i.e. terrestrial organic matter) (Arndt et al., 2013). Furthermore, some carbon isotopes are stable and do therefore not decay. Ultimately, however, the fraction of organic carbon avoiding degradation (and will thus end up in deep carbon cycling, (Arndt et al., 2006)) will be small (Canfield et al., 2005).

Furthermore, OM degradation rates have been shown to vary with seasons due to the temperature differences (Jørgensen and Sørensen, 1985). Degradation rates in colder areas differ, however, not necessarily compared to measurements in tropical sediments. These findings seem to contradict but can be attributed to the adaption of the bacterial community to the climate (i.e. a shift in the composition of the microbial community) (Robador A, 2009). However, the influence temperature has on the OM degradation rates is still difficult to estimate (Arndt et al., 2013). Additionally, it has been hypothesised that OM degradation rates are dependent on sediment accumulation rates. As the fresh OM effectively berries relatively older OM, it influences the older sediment's environment (Devol, 1998).

OM on the seafloor oxidates using Terminal Electron Acceptors (TEAs). These TEAs typically react with the OM in the order of O_2, NO_{3-}, Mn(VI), Fe(III) and SO_4^{2-} (Arndt et al., 2013). The preferred reaction is thus with oxygen.

Aerobic and anaerobic degradation

The microbial degradation under aerobic conditions, and thus with oxygen as TEA, releases CO_2. The half-reactions with oxygen and other Terminal Electron Acceptors, together with the half-reactions of the electron donor reactions, are given in appendix A. The sum of these gives the net redox reaction. Equation 2.4 is an example of the complete redox reaction of the oxidation of acetate by sulfate.

$$CH_3COO^- + SO_4^{2-} \rightarrow 2HCO_3^- + HS^- \qquad (2.4)$$

As can also be derived from appendix A, the microbial degradation under anaerobic conditions (i.e. without a oxygen supply), does not only release CO_2 (Yao et al., 1999, Zander et al., 2020, Arndt et al., 2013).

In anaerobic conditions, due to the decreasing redox potential and enthalpy, the organic carbon is first released from the reduction of TEAs like manganese, iron, nitrate and sulphate in the form of CO_2. Once these TEAs are depleted, the organic carbon will also be released as CH_4 (Zander et al., 2020). This part of the degradation process, called methanogenesis, is the terminal step of the OM degradation process (Gebert et al., 2006). Concurrently, all systems with anoxic bottom waters but high rates of OM sedimentation have a high CH_4 emission potential (Grasset et al., 2018). However, the rate of OM degradation decreases considerably faster in anaerobic than in aerobic conditions. It has been hypothesised that this is due to the catalysing enzymes being less active without oxygen present (Hedges and Oades, 1997). Furthermore, anaerobic degradation in sediments produces gas bubbles. These bubbles are assumed to delay sedimentation and consolidation, as well as decrease the viscosity, shear strength and density of the sediment (Zander et al., 2020).

In summary, the OM can degrade in three ways. The first and preferred manner is direct oxidation into CO_2. Secondly, the OM can be oxidised partly into intermediate compounds. Thirdly, the OM can be reduced to form CH_4. Which of these pathways the degradation process takes is dependent on conditions like deposition rate, macrobenthic activity, OM composition, electron acceptor availability, benthic community composition and physical protection (Arndt et al., 2013).

Besides the composition of the OM and oxygen availability, the carbon release rate is determined by several more factors. One factor which has shown statistically significant is the Total Nitrogen (TN) content (Gebert et al., 2006, Gebert et al., 2019).

Nitrogen

Several studies have shown the Total Organic Carbon (TOC) and TN to correlate significantly (Gebert et al., 2006, Yao et al., 1999). One reason for this is that its availability controls microbial activity and

growth. The TN has also been shown to correlate with the share of light OM (as a percentage of TOC) (Gebert et al., 2006). Furthermore, after oxygen, nitrate is the first electron acceptor reacting with the OM due to its electropositivity. This means, in theory, that the methanogenesis will only start after the depletion of nitrate (Gebert et al., 2006).

Though TN levels have a significant impact on the total amount of carbon released, only the chemical composition of the OM itself determines the actual degradability (i.e. the susceptibility to microbial degradation) (Gebert et al., 2019, Arndt et al., 2013).

Organo-mineral complexes

As stated earlier, young OM (like planktonic biomass) is broken down more easily by microbial degradation than older, heavier OM. One concept explaining this difference is the formation of organo-mineral complexes in older sediment layers. These organo-mineral complexes are more resistant to microbial degradation (Gebert et al., 2006).

With time, the OM continuously depletes while methane is produced and organo-mineral complexes are formed. As the OM available decreases the turnover of OM, production of methane and formation of organo-mineral complexes reduces significantly (Six and Paustian, 2014, Gebert et al., 2006).

In summary, the rate and magnitude with which OM degradation affects OM containing sediment thus depends on these factors:

- OM content; more TOC available will lead to more degrading OM.

- OM degradability ; sediment containing more easily degradable OM will be affected more compared to sediment containing organo-mineral complexes.

- Prevailing geochemical conditions; which electron acceptors are available.

- Prevailing environmental conditions; temperature and redox potential.

(Gebert et al., 2006, Arndt et al., 2013, Zander et al., 2020)

The samples this research means to analyse for their rheological properties have been, as stated in section 1.6, degraded by F. Zander. In this research (Zander et al., 2020), the sediment properties of degrading samples (i.e. some of the samples used in this research) have been thoroughly analysed and compared based on their spatial variability.

2.2.2. Degradation in the port of Hamburg

Generally, for more upstream sediments, F. Zander found a higher OM content, a lower TOC-TN ratio and higher concentrations of dissolved organic carbon in pore water (Zander et al., 2020). Concurrently, both the degradability and the mass-related release of carbon were higher for the upstream locations. The difference can be attributed partly to the higher amounts of easily degradable organic carbons (see section 2.2.1) found in the more upstream locations (Scböl et al., 2014). Per gram dry weight, the aerobically and anaerobically degraded OM showed a 10-30 and (up to) 10 fold increase, respectively. Also, the increased amount of nutrient concentrations at the upstream locations is likely to have a positive effect on these release rates (Zander et al., 2020).

However, following section 2.2.1, the strongest CH_4 production potential was found for the downstream locations. This can be attributed to the low availability of labile compounds at these locations (Grasset et al., 2018). In total, degradation under aerobic conditions releases three to five times more carbon than under anaerobic conditions (Zander et al., 2020). This could be explained by the less active catalysing enzymes in anaerobic conditions mentioned in section 2.2.1 (Hedges and Oades, 1997).

As the youngest OM gets transported to the harbour through the water body, the most freshly settled material is the least consolidated one. In these pre-consolidated layers, and thus with the highest water content, the OM is, therefore, least decomposed. Consequently, these low-density layers contain the highest amounts of TOC and TN (Zander et al., 2020).

More statistically significant correlations were found, including a strong relation between the TOC and the aerobically and anaerobically degradability of this carbon per unit TOC. This indicates that for samples with a high TOC concentration, a high percentage of this TOC can be expected to degrade.

Additionally, the expanding depletion of available pools in the samples over time correlated with reducing OM reactivity. This coincides with the decreasing degradation and redox potentials found with increasing depth (and thus age). Moreover, the TN and TOC contents and the TN/TOC ratios showed a strong positive correlation with the carbon release. The water temperature did not vary over the sampled locations (Zander et al., 2020).

This research aims to find more insights into what effect this degradation has on the rheology of the mud. The following section briefly explains why and how it plans to do this.

3

Methodology

For studying the rheological properties of the samples, a rheometer (Haake, MARS, ThermoFisher) is used. In previous research, A. Shakeel defined specific tests explicitly designed to test the mud for different rheological properties (Shakeel et al., 2020e, Shakeel et al., 2020b). As these tests have been performed on samples from the same location and the results have been conclusive, identical tests are conducted in this research.

Every sample will be subjected to five different tests, and a variety of rheological properties of these samples will be examined. The experiments will be done within 24 hours not to let the sample degrade further in uncontrolled conditions. Furthermore, the same temperature, stirring method, and overall test methodology are used to keep the number of changing variables to a minimum in the experiments. This way, it is certain the (possible) different results from the tests are due to the different properties of the mud under investigation. More detailed descriptions of the instruments and procedures used in this research are given in this chapter.

3.1. Samples

For this study, 129 'undisturbed' mud samples were taken from 11 locations of the port of Hamburg. These locations are shown in figure 3.1, in which the Elbe river flows from location ID J to K.

3.1.1. Location

A preliminary analysis was done on multiple locations in the area. The sites were selected because regular maintenance dredging is required at these locations. This is due to the sizeable fluid mud layer present. Furthermore, the selected locations have varying densities and OM contents. The associated names of the locations and abbreviations used in this research can be found in table 3.1. As mentioned in section 1.2.3, the TOC represents the total organic carbon content and is given in $\frac{\text{organic carbon [gram]}}{\text{dry weight [gram]}} * 100\%$. The coordinates of the locations are depicted in table E.1.

3.1.2. Sample preparation

The samples were taken using a 1m core sampler, shown in figure 3.2. Five mud layers were defined; fluid mud (FM), fluid mud to pre-consolidated mud (FM/PS), pre-consolidated mud (PS), pre-consolidated to consolidated mud (PS/CS) and consolidated mud (CS). The lutocline, the upper boundary of the FM layer, was visually identified and seconded by density measurements onboard (Anton Paar density meter DMA 35) (Zander et al., 2020). The depth of every layer was determined based on the visual consistency and their distance to the lutocline. The separated layers were transferred to a laboratory in cooled, air-tight containers.

A 'fresh' sample was separated for all layers and locations and tested for the rheological properties within 48 hours. The identical counterparts of these 'fresh' samples were then used for a study on the degradation of organic matter under aerobic and anaerobic conditions (Zander et al., 2020). Furthermore, identical samples were degraded aerobically and anaerobically for 250 days. During these

Location	Location ID	Average TOC [%]	Distance from the Elbe river [km]	In figure 3.1
Köhlbrand	KB	3.5	623	E
Rethe	RT	4.1	619	B
Reiherstieg Vorhafen	RV	6.2	616	A
Köhlfleet mit Köhlfleethafen	KH	3.8	629	H
Sedimentfang Wedel	SW	2.7	643	I
Parkhafen	PK	3.5	627	G
Oortkaten	OK	7.0	607	F
Dove Elbe	DE	3.9	615	D
Zollenspieker	ZS	4.7	599	J
Lühesand	LUS	unknown	651	K
Au(ringels)eneste	AE	unknown	635	C

Table 3.1: A overview of the sample locations.

degradation processes, the gas production rates were monitored (Zander et al., 2020). After these degradation processes, the samples were tested for their rheological properties within 48 hours. Just before testing, the samples were homogenised. The homogenisation was done by stirring the sample thoroughly with a spoon until the sample looked homogeneous (approximately 30 s).

3.1.3. Density measurements

As a final step before testing, a part of each (homogenised) sample is poured into a cup, weighed and put in the oven. After approximately 24 hours at 100 degrees °C, these cups are removed from the oven and weighed again. By then, all water is evaporated, leaving only the minerals. The dry density was assumed to be 2650 kg/m^3 (Coussot, 2017). Knowing the weight of the solid mass and the water removed, the densities of the samples were calculated as described by (Coussot, 2017).

3.2. Rheometer

The rotational rheometer, HAAKE MARS I, used in this research is depicted in figure 2.2. This model is a shear stress-controlled rheometer, as explained in section 2.1.1, but is also able to perform shear rate based experiments using a feedback loop. In order to measure a sample, a geometry needs to be attached to the rheometer. This geometry will then be (partially) submerged in the cup filled with the sample, after which the desired measurements can take place.

3.2.1. The geometry

This geometry can have different shapes and sizes, with their own pros and cons. In this research, the Couette (or bob) geometry is used, shown in figure 3.3a. The Couette geometry (a concentric cylinder) can struggle with wall-slip at low shear rates or shear stresses, while others (like the vane geometry) do not. However, a Couette geometry can better show a two-step yielding curve of fluid mud at higher shear rates. As the structure within the mud will be destroyed soon at these rates by a vane geometry (Shakeel et al., 2020f).
Additionally, with a Couette geometry, there is only a tiny gap between the bob and the wall of the cup. This leads to a linear velocity profile in the mud, simplifying calculations. Accordingly, previous research has shown that the Couette geometry is the best fit for the experiments conducted in this research, as it is the most suitable for analysing both yield stresses for the samples (Shakeel et al., 2020e).

Therefore this research was performed using a Couette geometry (CC25 DIN Ti). The distance from the bottom of the cup was 5,3 mm with a gap width of 1 mm. Appendix B gives a brief overview of the formula's used to obtain the shear stress σ and shear rate $\dot{\gamma}$ using this geometry.
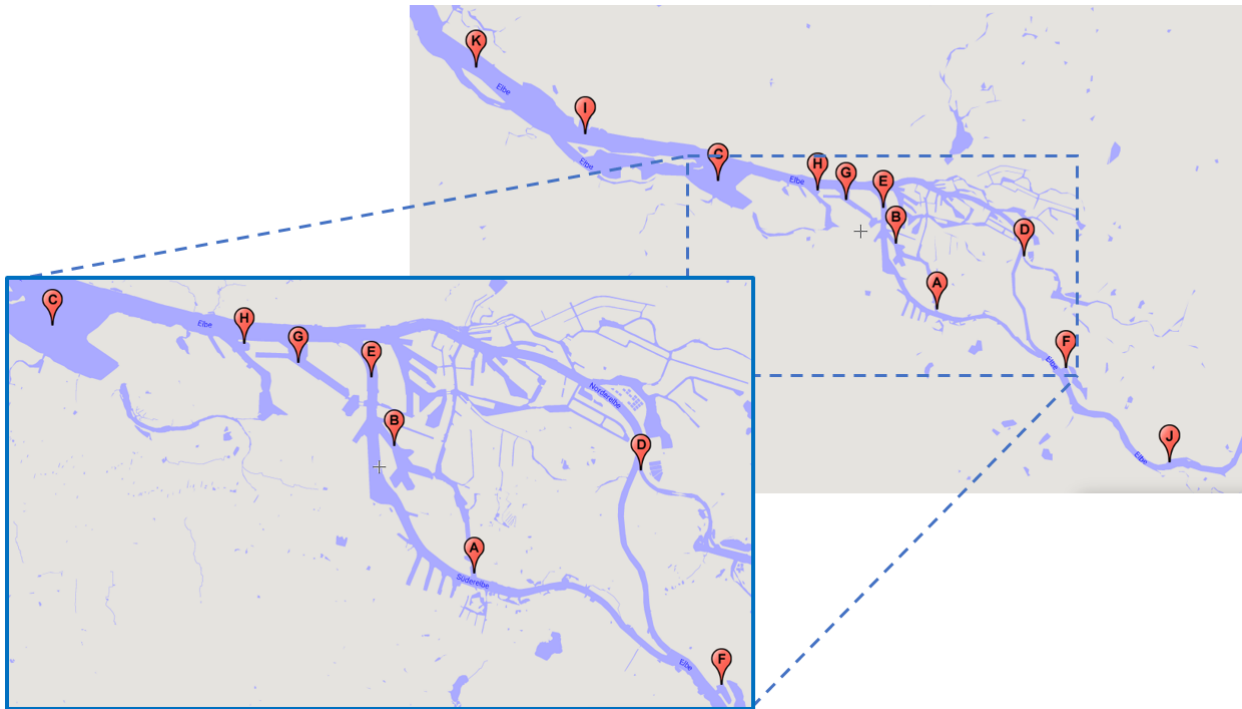
Figure 3.1: The sample locations on a map of the port of Hamburg's waterways.
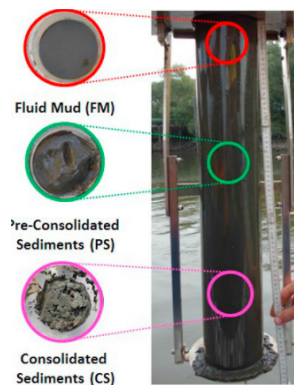
Figure 3.2: Mud sediment sample collector. Taken from Shakeel et al., 2020a.

3.3. The protocols

Tailored measurement protocols must be constructed to derive rheological properties from the samples. The protocols executed in this research have been described and used in preliminary research with precise results (Shakeel, Kirichek, et al., 2019, Shakeel et al., 2020b).

During the experiments, the temperature was controlled using a Peltier controller and maintained at 20 degrees °C at all times. At the start of each test, a waiting time of 30 s was programmed after the bob attained its measurement position. Therefore, the disturbance in the sample caused by the bob is somewhat mitigated. Furthermore, the protocols used in this research were duplicated frequently to test the repeatability of the results. The procedures followed in each experiment are provided in detail in the following sections.

3.3.1. Stress sweep

After the 30 s waiting time, the applied shear stress, τ, is linearly raised from zero to a set value with an increased rate of 0,1 to 1 N/m^{2}s. The set value and increase rate are chosen each time, depending

(b)
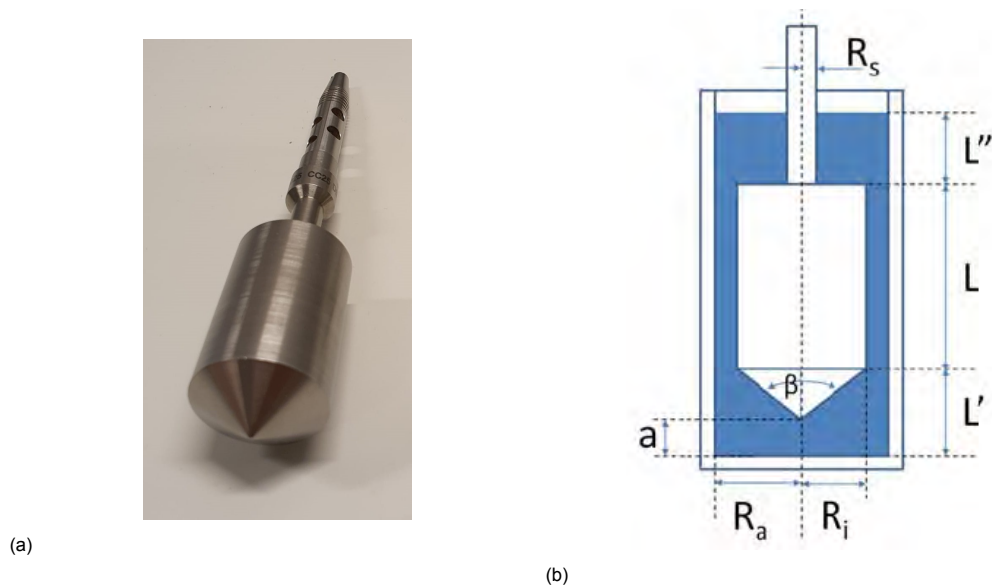
Figure 3.3: The Couette geometry (l) and a schematic depiction of the Couette geometry. Taken from *HAAKE MARS Rheometer Instruction Manual*, 2014 (r).

on the sample's apparent consistency. Every 0.5 s, the shear rate, $\dot{\gamma}$, resulting from the applied shear stress, is measured. Then when $\dot{\gamma}$ has reached 300 s^{-1}, the experiment halts. This time-saving limitation is in place because we observe 2 step yielding before it, and the data obtained after this speed will thus not be used regardless.

Furthermore, the yield stresses ought to be apparent from the data at this point. The stress sweep is plotted with τ on the x-axis and on the y-axis. Additionally, the static- and fluidic yield stresses are determined as discussed in section 2.1.3. The stress sweep was performed twice on every sample because the yield stresses are of great interest to this research. Whenever the two results would yield different unsatisfactory results, a third test was performed to provide additional direction in determining the genuine yield stresses. As little sample was available for the aerobically degraded samples, only one stress sweep was conducted (if the sample size was sufficient) on these samples.

3.3.2. Oscillatory amplitude sweep

The oscillatory amplitude test applies increasing sinusoidal stress to the sample (after the 30 s waiting time). The frequency was chosen to be 1 Hz, as preliminary research found this to be the most suitable for identical samples (Shakeel et al., 2020e). By taking the resulting strain γ, the storage modulus G' and loss modulus G'' are determined using equation 2.2. As discussed in section 2.1.3, these moduli represent the in-phase and out-of-phase responses of the material, respectively.

The amplitude sweep results are plotted with the increasing stress on the x-axis and G' and G'' on the y-axis. A point of interest in this data is the "cross-over amplitude". This is the amplitude, in [Pa], from where G'' is higher than G'. This amplitude is of interest since the transition from elastic to viscous happens at this stress level.

The cross-over amplitude completes an explicit estimation of the linear viscoelastic regime. This information is used to determine the next experiment; the frequency sweep.

3.3.3. Frequency sweep

After the 30 s waiting time, a oscillating shear stress is applied on the sample with a predetermined amplitude. As the name suggests, this oscillating stress is then applied with increasing frequency. The stress chosen is based on the results of the amplitude sweep and tuned to still be within the linear viscoelastic regime for each sample. From 0.1 to 100 Hz, G' and G'' are measured.

With this method, the applied stress is relatively small and only for short periods. Therefore, γ stays very small. This means the sample is not disturbed while testing. This is important, as the stress might

otherwise exceed the viscoelastic regime, invalidating the results.

The complex modulus G^* and phase angle δ can then be determined using formulas 3.1 and 3.2. The system's consistency can be measured with the complex modulus, whereas the phase angle represents the level of structuration.

$$G^* = \sqrt{G'^2 + G''^2} \tag{3.1}$$

$$\delta = \tan^{-1} \frac{G''}{G'} \tag{3.2}$$

The resulting G^* and δ values are then plotted on the y-axis with the applied frequencies on the x-axis. Two frequency sweeps are conducted for fresh and degraded samples to validate the results. This extra check is done because two frequency sweeps of the same sample can have substantial differences, which will further be investigated when detected. Since comparing graphs for all samples would be highly time-consuming for this research, only the G^* and δ values at 1 Hz are compared for simplicity.

3.3.4. Thixotropic loop

In the thixotropic loop experiment, the shear rate $\dot{\gamma}$ is, after the 30 s resting time, first ramped up from 0 to 100 s^{-1}. This increase happens linearly over 50 s. Then $\dot{\gamma}$ is held constant at 100 s^{-1} for 50 s, and after that, taking 50 s decreased back to zero again. A hysteresis loop is then obtained from this test, which can be compared for different samples. More information on the thixotropic loop has been given in section 2.1.3.

3.3.5. Structural recovery test

The protocol used in this research is constructed as explained in (and described extensively in) Shakeel et al., 2020a, and shown in figure 3.4.

The protocol starts by applying oscillating stress with amplitudes between 0,1 and 1 Pa (always within the linear viscoelastic regime) for 100 s. Then, the storage modulus (before the structural breakup), G_0', is measured. Because of the small stress applied, little shear will take place the sample will thus not be disturbed significantly, as explained in section 3.3.3. As shown in figure 3.4, the last value for G' measured is the storage modulus before structural breakup; G_0'. The initial structure of the mud is at this state still intact, as shown in figures 3.4 and 2.6.

Then the sample structure is broken by applying a shear rate $\dot{\gamma}$ of 100 s^{-1} for 500 s. Subsequently, the structural recovery phase starts. In this phase, G' is measured again by applying oscillating stress with an amplitude within the linear viscoelastic regime (between 0,1 and 1 Pa). The first G' measured is named the storage modulus after the structural breakup; G_i'. The structure will likely recover since the small oscillating stress does not further disrupt the mud. As the time, t, approaches ∞, G' will converge to G_∞'. The experiments in this research are performed for 500 s in the structural recovery phase.

The results of the structural recovery test are plotted with time t on the x-axis, with t=0 as the start of the structural recovery, as shown in figure 3.4. On the y-axis, G' over this period is divided by the sample-specific constant G_0'.

G_∞' can not be obtained directly from the gathered data. Therefore, equation 3.3 is used to fit a curve over the data (equation from Mobuchon et al., 2007 and Mobuchon et al., 2009). In this formula, t, G', G_0', G_i' and G_∞' are defined as explained above. Additionally, t_r is the characteristic time of the material, reflecting the time needed for the sample to reach 63 per cent of G_∞'. Furthermore, d is a stretching component that lies between 0 and 1. A small d reflects an initially fast recovery followed by a slower recovery in later stages (Shakeel et al., 2020e). The fitting parameters used are thus G_∞', t_r and d, as all others could be obtained from the data.

$$\frac{G'}{G_0'} = \frac{G_i'}{G_0'} + \left(\left(\frac{G_\infty' - G_i'}{G_0'} \right) \left(1 - \exp\left[-\left(\frac{t}{t_r} \right)^d \right] \right) \right) \tag{3.3}$$
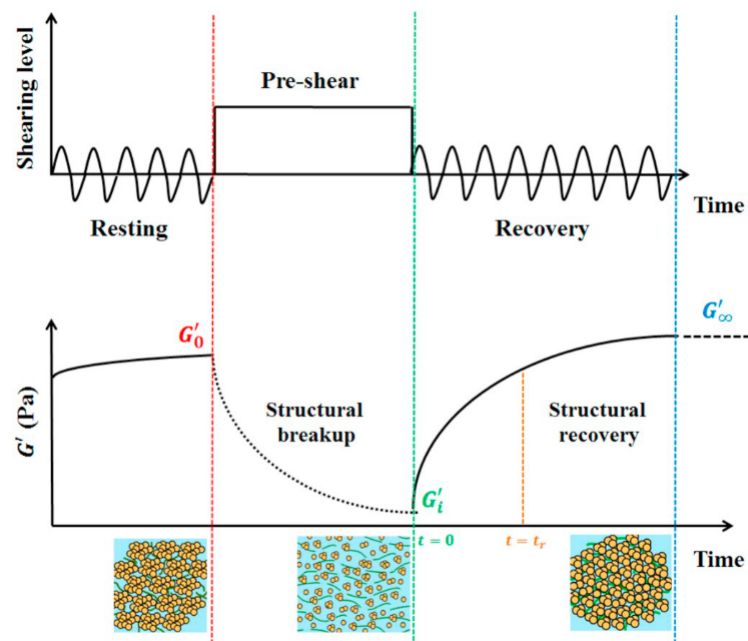
Figure 3.4: A schematic depiction of the experimental protocol of the structural recovery test. Taken from Shakeel et al., 2020a.

<div style="text-align: right; font-size: 4em;">4</div>
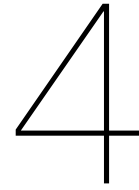
Results and discussion

A total of 129 samples have been tested using the methods discussed in the previous chapter. For each of these samples, the fresh and degraded subsamples have been subjected to the tests as described there. As the characteristics of these samples vary in multiple aspects simultaneously (density, TOC amount, location and seasonality), noise in the data is observed when all samples are compared at once. For this reason, smaller groups of data are selected, differing on the variable under investigation. An overview of all obtained data is available, as explained in appendix D.

4.1. Plotting

To properly compare the results, the plotting has to be done consistently. This section explains the used plotting methods in more detail. For each of the protocols discussed in section 3.3, a depiction of the resulting graphs is given below.

4.1.1. Stress sweep

The stress sweep is plotted with the shear stress τ on the x-axis and viscosity on the y-axis, as shown in figure 4.1. As can be seen, the static and fluidic yield stresses of the anaerobically degraded sample are significantly lower than those of the fresh sample. For this sample, the degradation of the organic matter thus weakens the mud significantly.

In order to enable meaningful comparisons in a large amount of data gathered, the static- and fluidic yield stresses of all samples are determined as depicted in figure 4.1 (and discussed in section 2.1.3). The yield stresses of all samples have been determined manually in this manner.

4.1.2. Oscillatory amplitude sweep

The amplitude sweep results are plotted with the increasing stress on the x-axis and G' and G'' on the y-axis, as depicted in figure 4.2. As described in section 3.3.2, a point of interest in this data is the "cross-over amplitude". From this amplitude upward, the sample behaves more viscous than elastic manner. A decrease of this cross-over amplitude after degradation thus also implicates that the sample has gotten weaker. The cross-over amplitudes were determined from the data using the Matlab script depicted in figure C.1.

4.1.3. Frequency sweep

With the frequency sweep, the values for the complex modulus G^* and phase angle δ are plotted against the applied frequencies, as depicted in figure 4.3. As shown, the fresh and anaerobically degraded sample vary in G^*, but behave alike against the frequencies. Therefore the differences in the results can be represented quite accurately by taking G* at 1 Hz and comparing these values with one another.

A decrease in the complex modulus at 1 Hz, like sample 17201, indicates a decrease in the overall resistance to elastic- and fluidic deformation. The phase angle indicates the relation between these
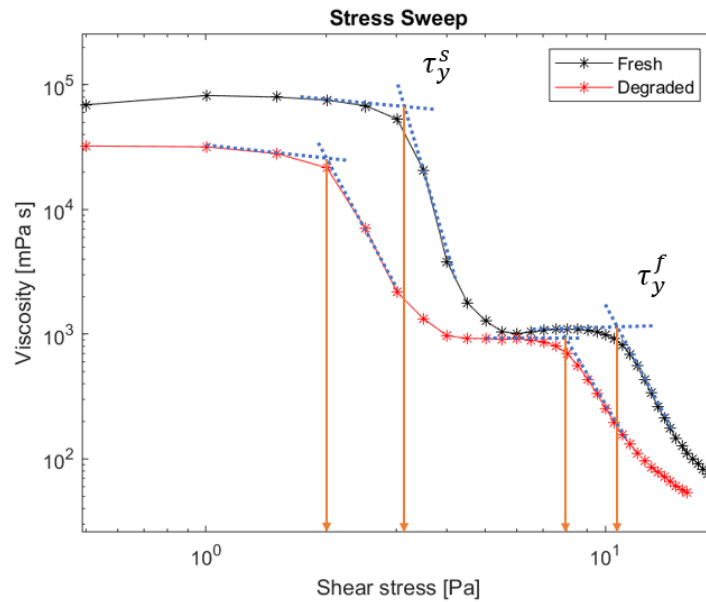
Figure 4.1: An example of the plotted results from two stress sweeps performed on sample 17203; one before (black) and one after degradation (red). The blue and orange lines represent the method used to determine the static and fluidic yield stresses.

two, as can be seen from equations 3.1 and 3.2. As with the example in figure 4.3, most phase angles found in this research lie between 8 and 10 degrees, with an average of 9,58. A phase angle under 45° implicates $G' > G''$, meaning the sample has a predominantly elastic reaction to a 1 Hz oscillating stress. As the stresses applied in the frequency sweeps were chosen within the viscoelastic regime of the sample (see section 3.3.3), all phase angles found in this research are < 45°.

4.1.4. Thixotropic loop

In the thixotropic loop experiment, the shear rate $\dot{\gamma}$ is first ramped up from 0 to 100 s^{-1}. Then $\dot{\gamma}$ is held constant at 100 s^{-1}, and after that decreased back to zero again. The results of this experiment are plotted with the shear stress on the y-axis and the shear rate on the x-axis. The results for sample 15206 are given in figure 4.4.
The clockwise loop formed in figure 4.4 is called the hysteresis loop. When the hysteresis loop is bigger, the 100 seconds of constant shearing has had a relatively large effect on the rheology of the mud. Therefore, comparing these surfaces can give additional insight into the effect of degradation on the rheology. For this reason, the surfaces of all hysteresis loops have been determined using the Matlab script shown in figures C.2 and C.3.

4.1.5. Structural recovery

The results of the structural recovery test are plotted with time t on the x-axis, with t=0 as the start of the structural recovery, as shown in figure 4.5 (Shakeel et al., 2020e). On the y-axis, G' over this period is divided by the sample-specific constant G_0'. The results of sample 18210 are given in figure 4.6 as an example. The curves plotted over the data are the fitted relations from equation 3.3, as described in section 3.3.5 (Mobuchon et al., 2007, Mobuchon et al., 2009).
These fittings have been executed using the Matlab code shown in figure C.4. The resulting values for G_∞', t_r and d for all samples are available through appendix D. The structural recovery can therefore be quantified by the difference between G_∞' and G_0'. G_∞'/G_0' will be the fraction used in this research to compare different samples. Additionally, the t_r values will be compared, as these give complementary information on the recovery process.
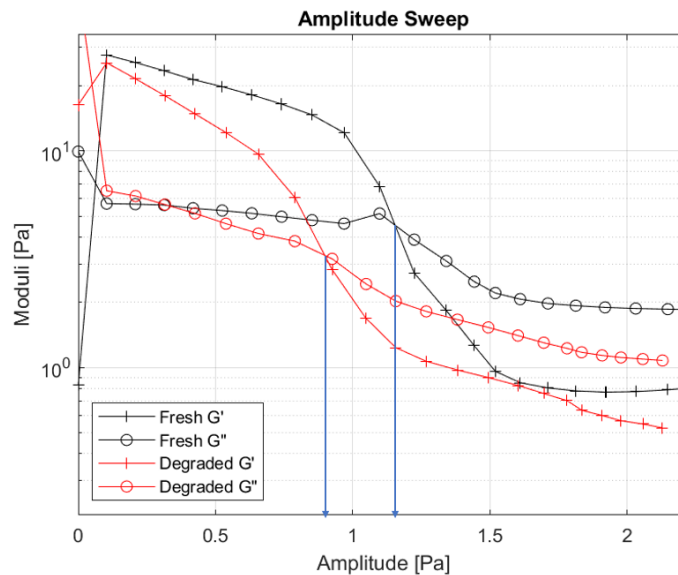
Figure 4.2: An example of the plotted results from two amplitude sweeps performed on sample 18207; one before (black) and one after degradation (red). The blue lines represent the method used to determine the cross-over amplitudes.

Rheological parameter	Definition
Static yield stress (τ_y^s)	The applied stress required to initiate the flow of mud.
Fluidic yield stress (τ_y^f)	The applied stress beyond which the mud will flow even more freely.
Cross over amplitude	The transition point from solid-like to liquid-like (G″ = G′).
Hysteresis loop surface	Difference between the stress before- and after shearing.
Complex Modulus G^*	Overall resistance to deformation without disturbance.
Structural recovery fraction G_∞'/G_0'	The fraction of strength the mud will recover after a period of shearing
Structural recovery time t_r	The time the sample takes to get to 65 % of G_∞'.

Table 4.1: A summarizing overview for the rheological parameters under consideration.

4.2. Comparing the results

This research aims to find the effect of degradation on the rheology of natural mud. Therefore, the differences between the degraded and the fresh samples are under investigation. For clarity, the table 4.1 provides a quick overview of the rheological parameters described in the previous section.

A first look into the effect of density on the rheological properties could be given by figure 4.7. Here, for each sample, the τ_y^f of the fresh sample has been subtracted from the (anaerobically) degraded sample. Clearly, the τ_y^f generally decreases after degradation. Furthermore, $\tau_{y_{degraded}}^f - \tau_{y_{fresh}}^f$ (i.e. the absolute change) seems to be inversely related with the density of the fresh sample. These results will be further discussed in section 4.3.1.

Several properties that might influence the effect of degradation on rheological behaviour are of interest. However, each sample measured has a unique combination of these properties. This results in much noise when plotting the results of the whole data set. Therefore, to say anything meaningful about the data, some groups of samples have been selected to investigate each research question separately. In this example, investigating the density, the five mud layers defined can be used; FM, FM/PS, PS, PS/CS and CS. This can be plotted in a box plot, seen in figure 4.8a. The settings of all box plots presented in this research are as follows; X mark = mean, line = median, box = 25th-75th percentile, upper whisker = highest data point within 1,5IQR of the 75th percentile, lower whisker = lowest data point within 1,5IQR of the 25th percentile (IQR; interquartile range = 75% - 25%).

As the density increases, a clear downtrend is visible. This trend is not surprising as the fluidic yield stress is known to be positively correlated with the density (Shakeel, Kirichek, et al., 2019). In order to filter this trend out of the results in further investigations, the y-axis can be divided by the shear stress
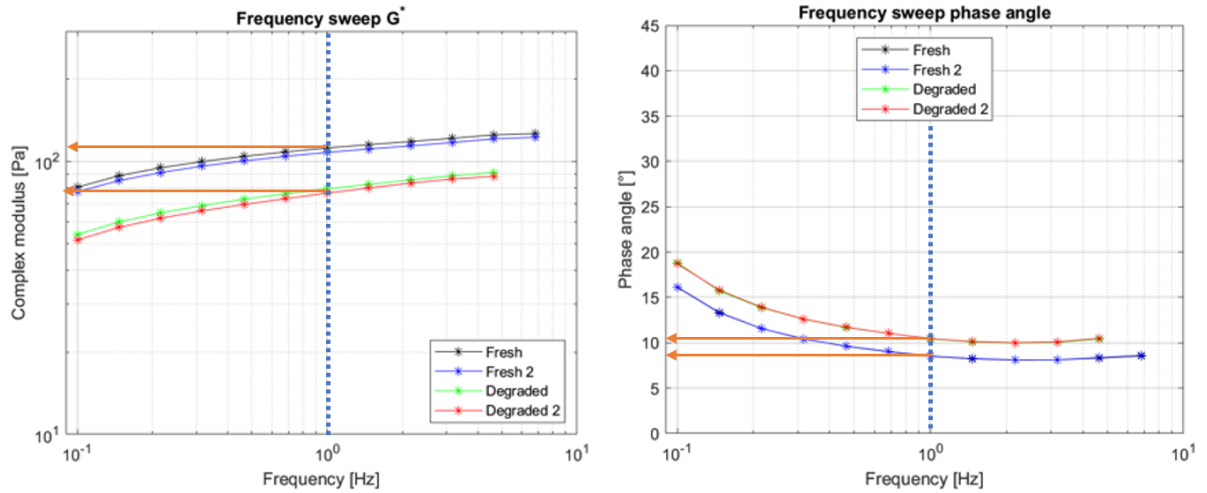
Figure 4.3: An example of the plotted results from four frequency sweeps performed on sample 17201; two before (black and blue) and two after degradation (green and red). The blue and orange lines represent the method used to determine the complex moduli and phase angles at 1 Hz.
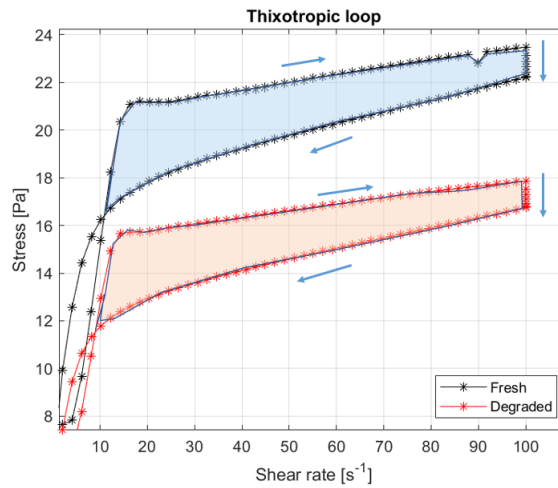
Figure 4.4: An example of the plotted results from two thixotropic loops performed on sample 15206; one before (black) and one after degradation (red). The blue and orange surfaces represent the hysteresis loops of the fresh and degraded sample respectively. The arrows represent the chronological order in which the data points were collected.

of the fresh sample. This results in figure 4.8b. Further results will frequently be shown in this form (the relative yield stress difference), as it is a good representation of the relative effect of the degradation on the concerning parameter. The results of this particular graph will be discussed in section 4.3.1.
With these box plots, the results will be used to answer the research questions defined in section 1.5.

4.3. The effect of density

For the first research question, the influence of density on the effect degradation has on the rheology is sought. As discussed, only an increasing difference in τ_y^f between the samples with density can be seen in figure 4.7. Except for G_∞'/G_0' and tr, this trend is also visible for the other parameters, as can be seen in figure E.2.
Furthermore, the samples are thus grouped by mud layer and plotted with (degraded-fresh)/fresh on the y-axis. The τ_y^f box plot is given in figure 4.8b and the results of the other parameters are depicted in figure E.3. No clear trends are visible.
The graphs displayed so far include the results of all samples tested and thus with different TOC con-
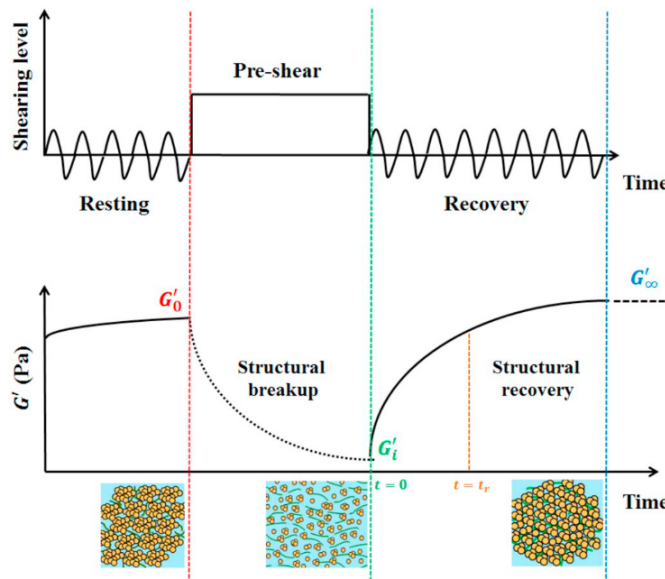
Figure 4.5: A schematic depiction of the experimental protocol of the structural recovery test. Taken from Shakeel et al., 2020a.
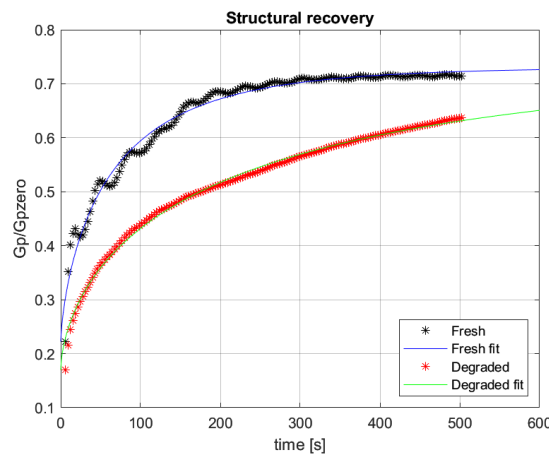
Figure 4.6: An example of the plotted results from two structural recovery tests performed on sample 18210; one before (black) and one after degradation (red). The blue and green lines represent the model fitting.

tents. As shall be seen in section 4.4, this also exerts influence on the results. In order to filter out this influence, the results of the individual locations are looked at separately. The locations Rethe (RT) and Köhlhafen (KH) were investigated first, as many samples have been gathered from these sites. The box plots with fluidic yield stresses for these locations are depicted in figure 4.9. The plots of the other parameters of locations RT and KH are shown in figure E.4 and E.5 respectively. For location RT a trend seems to be present; the degradation in denser mud layers seem to have more effect on the rheology than less dense layers. Interestingly, this trend is not visible for location KH. These differences will be discussed in the following section.

Additionally, the yield stresses of location RV are given in figure 4.10. The location RV is of interest as this location is not dredged regularly. Furthermore, the box plots for the fluidic yield stresses of the other locations are depicted in figure E.6.

4.3.1. Discussion

Looking at the results in figure 4.7 and E.2, the degradation clearly affects the rheological properties of the samples. The samples for which the τ_y^f, τ_y^s, cross-over amplitudes, G^* and hysteresis loop surfaces decrease after degradation outnumbers the samples for which these increase. This corroborates the
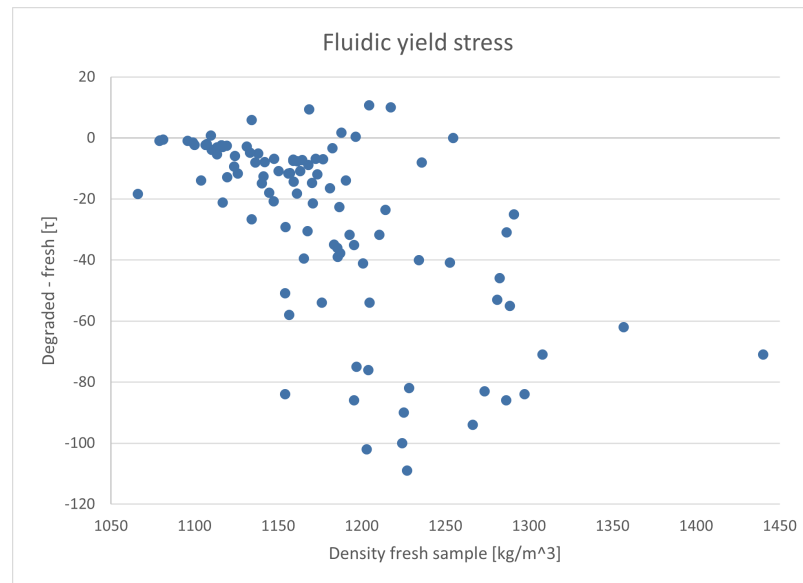
Figure 4.7: All τ_y^f of the anaerobically degraded sample minus their fresh counterparts plotted as a function of the density of the fresh samples.

expectations from earlier research (Shakeel et al., 2020c). Furthermore, a positive correlation between the magnitude of the difference between the degraded and fresh sample and the density is visible, with more dense samples displaying higher yield stresses and other properties. The degradation effect seems to be a certain fraction of the original properties. This positive correlation is not visible for G_∞'/G_0' and tr. This will be explained in section 4.8.

The density depending trend is thereafter eliminated by dividing the difference by the result from the fresh sample. The resulting graphs, figure 4.8 and E.3, do not showcase any clear trends between the mud layers. This is interesting because there are some reasons to expect a positive- and some reasons to expect a negative correlation with the increasing density.
One phenomenon that could cause a negative correlation is the different OM types between the layers. Low-density layers like the FM layer contain relatively more light fraction OM while having similar TOC contents. As light fraction om is more susceptible to degradation (Gebert et al., 2019), as elaborated in section 2.2.1. Furthermore, the preferred TEA's (oxygen and nitrate) are more readily available in the FM layer. For these reasons, a higher % OM turnover is expected for these layers. This has been observed for the investigated samples by earlier research (Zander et al., 2020).

A reason to suspect a negative correlation would be the samples' different absolute amounts of OM. While the TOC% of the layers is similar, this percentage represents the mass percentage of the dry weight. Moreover, as the dry weight of the denser mud layers is higher than the dry weight of the less dense samples, this means there is more TOC present in the denser mud layers. The fluid samples thus contain smaller amounts of TOC, but the TOC they do contain is more degradable than the TOC of the less fluid samples. The dense samples have a larger amount of TOC, but this TOC degrades relatively slow.

Another explanation for a positive correlation could be the air pockets in the more dense layers. As the OM degrades, several gasses are produced, like CO_2 and CH_4. In anaerobic conditions, this can cause gas bubbles (Zander et al., 2020). Though the samples were homogenized before testing, some of these gas bubbles could still be present in more dense samples while testing. If these gas bubbles are present, they could reduce the strength of the mud (Zander et al., 2020) and lead to a positive correlation.
As the results indicate no correlation, the effects of the phenomena described seem to be in balance. In the next section, the same results for individual locations will be compared to gain additional insight into these influences.
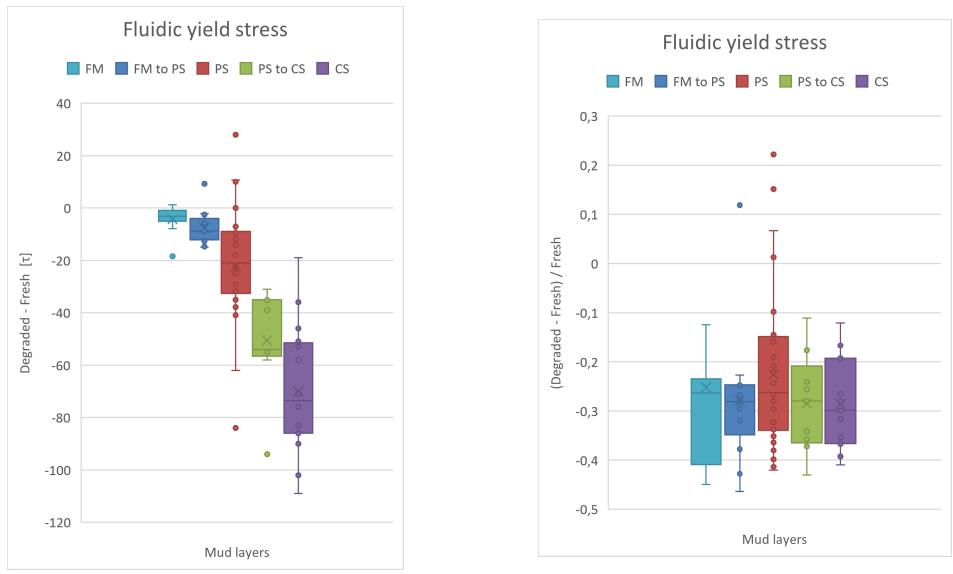
Figure 4.8: All τ_y^f of the anaerobically degraded sample minus their fresh counterparts for all locations, sorted by mud layer (a). Then divided by the fresh results in (b).
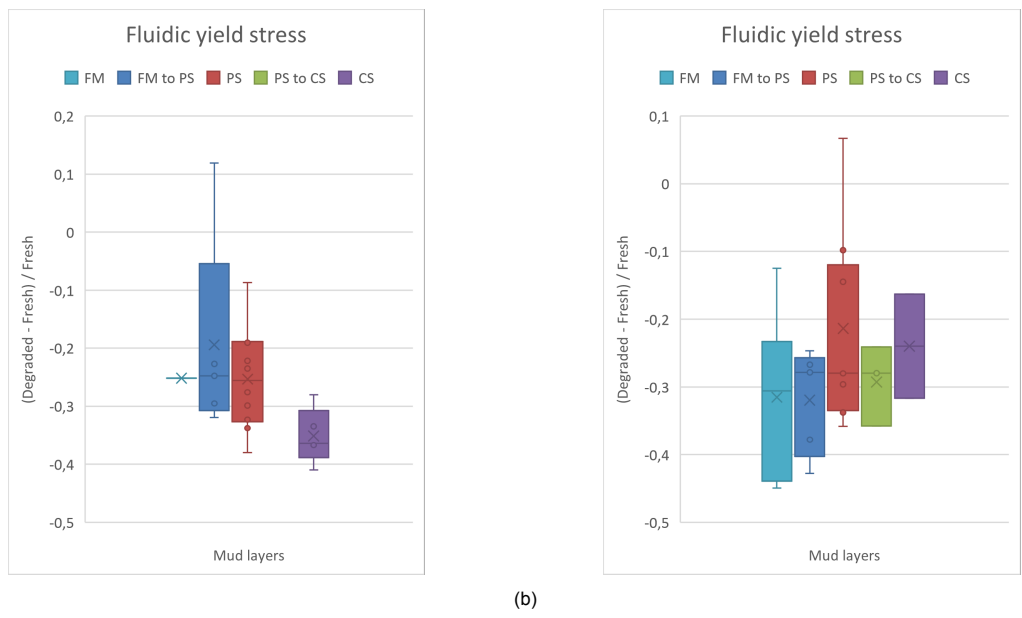
(a)

(b)

Figure 4.9: Box plots of the relative differences of τ_y^f for location RT (a) and KH (b), grouped by mud layer.

(a)   (b)
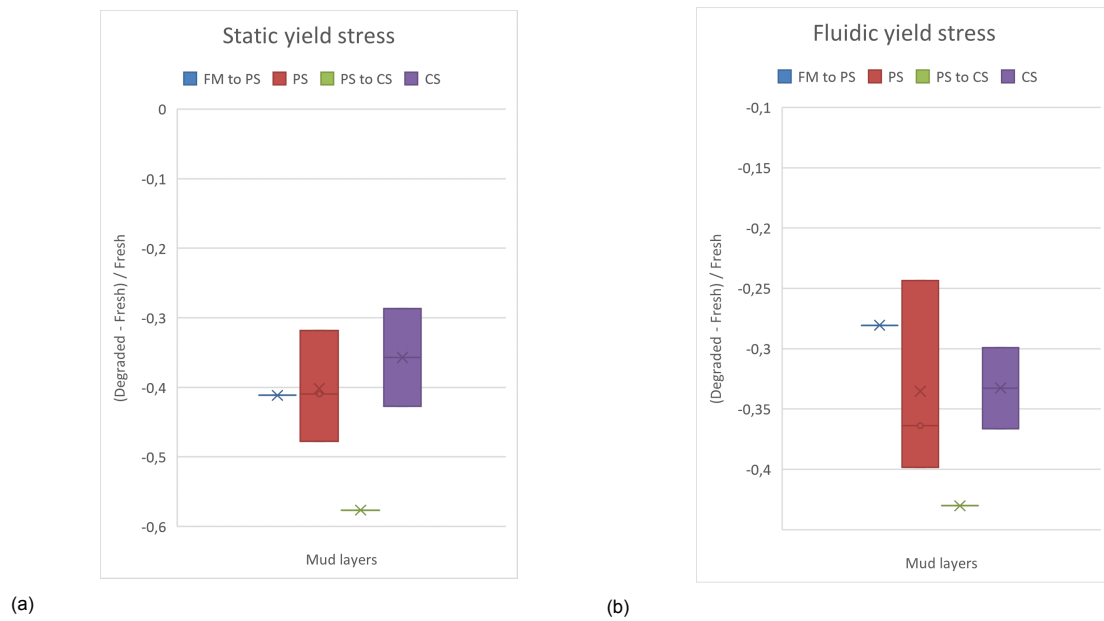
Figure 4.10: Box plots of the relative differences of τ_y^s (a) and τ_y^f (b) for location RV, grouped by mud layer.

Locations

The difference in the effect of degradation on different mud layers between the locations RT and KH is surprising as the TOC contents are very similar. One reason for this trend could be that location KH is frequently subjected to water injection maintenance dredging. The settlement structure could therefore be different. Another difference between KH and RT that could have an effect is the light organic matter content. The location RT is upstream from KH, and the influx of light fraction TOC transported with the river from its catchment could therefore be more significant. The degradation of the OM at the time of sampling could also be different due to the water injection dredging process.

The only location where negative correlation is also visible is location KB, next to RT. Other locations, however, like RV, ZS and OK, lie even more upstream. And while little data is collected from these locations, the results do not point towards a heavier inverse correlation for more upstream locations (see figure E.6).

4.4. The effect of TOC content

The scatter diagrams with the degraded-fresh or (degraded-fresh)/fresh results, shown in figure 4.11, do not clearly indicate any trends relating τ_y^f with the TOC %. Only when a trend line is added to the figure on the right, a trend can vaguely be observed. Therefore, three locations with significant TOC differences are compared. The locations with enough samples to lead to a meaningful result were Sedimentfang Wedel (SW), Rethe (RT) and Reiherstieg Vorhafen (RV). The average TOC contents for these locations are 2,7%, 4,1% and 6,2% respectively. The fluidic yield stresses for these locations are shown in figure 4.12. The box plot results for the other parameters are depicted in figure E.7.

No clear trend can be identified from the scatter diagrams in figure 4.11. Once only the three locations are plotted in figure 4.12 however, a trend does show. The same trend is observed with the τ_y^S, cross-over amplitudes, G^* and hysteresis loop surfaces in figure E.7. The impact of the degradation on the rheological parameters is positively correlated with the TOC content of the samples. Again, G_∞'/G_0' and t_r do not show the same trend.

Additionally, the effect of TOC % is looked at for different densities. First, all samples (for which the TOC is known) are divided in three groups based on densigy; (1) all samples with $\rho < 1100[kg/m^3]$, (2)
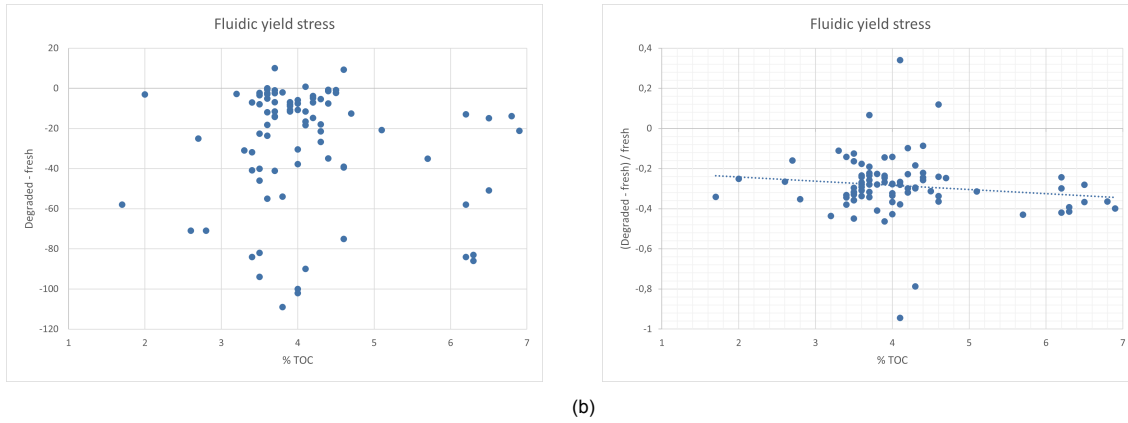
(a)

(b)

Figure 4.11: All τ_y^f of the anaerobically degraded sample minus their fresh counterparts plotted against the density of the fresh samples on the left and the same but divided by the fresh sample on the right.

(a)

(b)
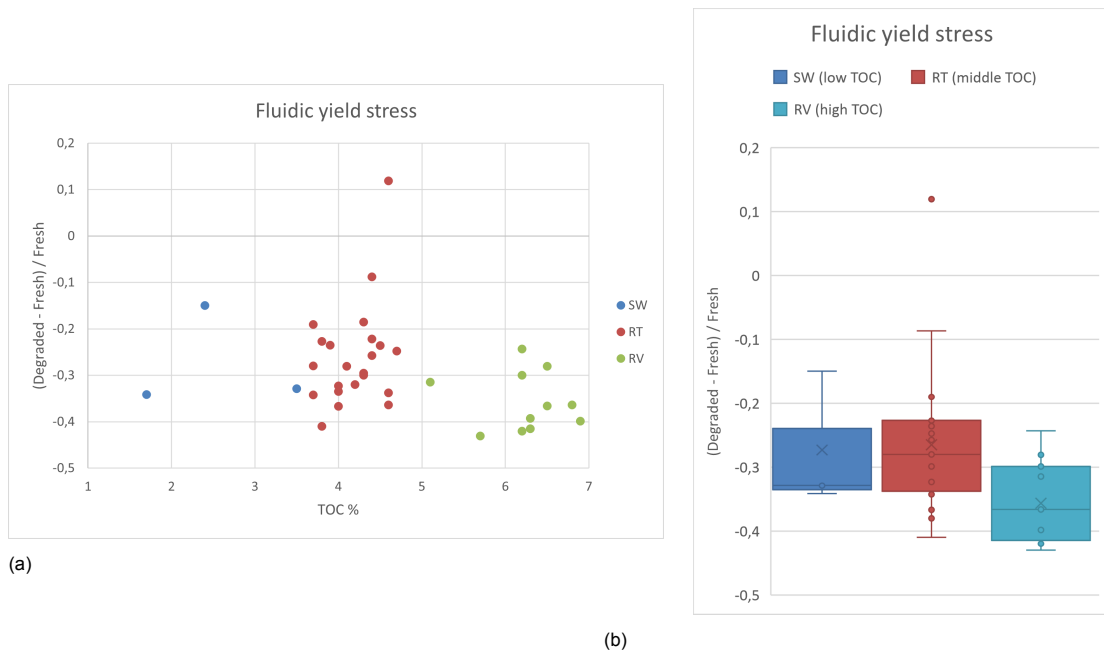
Figure 4.12: The τ_y^f results for the locations SW, RT and RV. Depicted in a scatter diagram on the left and a box plot on the right.
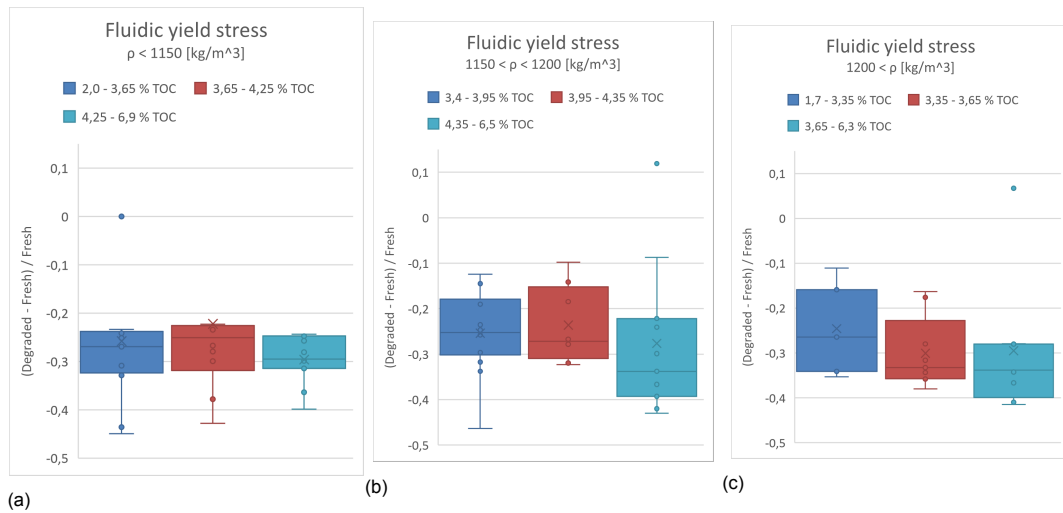
Figure 4.13: The τ_y^f results for all locations. The samples with lower, middle and higher densities in (a), (b) and (c) respectively, grouped on TOC contents.

all samples with $1150 < \rho < 1200[kg/m^3]$ and (3) all samples with $1200 < \rho[kg/m^3]$. Subsequently, these groups were divided into three subgroups based on their TOC %. The box plots comparing these subgroups for each density group are depicted in figure 4.13.

4.4.1. Discussion

As expected in section 1.5, figures 4.11 and 4.12 indicate that the impact of OM degradation on the rheology is indeed dependent on the TOC content (in mass percentage) in the samples. The impact of the degradation is positively correlated with the TOC % of the locations for the τ_y^f, τ_y^s, cross-over amplitudes, G^* and hysteresis loop surfaces.

Figure 4.13 provides additional insights; while the correlation described above is barely visible for low-density samples, it increases strongly with the density. In line with figures 4.8 and E.3, figure 4.13 does not show a bigger average effect for a certain density group. Only a clear difference of the effect of the TOC % between these groups. This result could have several reasons. Firstly, as mentioned in section 4.3.1, the TOC % in the high-density samples could have more effect because this TOC % represents more absolute TOC (due to the high density). Furthermore, the difference in density also means that the denser samples have significantly more particle interaction. Therefore, if a certain percentage of these closely packed particles is removed, this could have bigger consequences for the structure of these denser layers.

4.5. The degradability

In order to answer the sub-question on the effect of the degradability of mud, the samples compared would ideally be identical in all other aspects. However, as they are collected in situ, the samples tested in this research differ in TOC content, density, date collected, and other ways. Furthermore, the TOC % is positively correlated with the degradability in the samples (as shown in table 4.2). Finding a direct trend between rheological parameters and degradability is therefore complicated.

In figure 4.14a, the relative fluidic yield stress differences are plotted for the locations SW, KH, RT and RW. These locations were selected as they vary in degradability (see table 4.2). Furthermore, the TOC % are plotted as a function of degradability for these locations in figure 4.14b.

Additionally, a recent study indicated that the effect of degradation on rheology happens in the first few days after removing the sample from in situ conditions (Zander et al., 2022). Therefore, a box plot on the mg carbon / g TOC after 21 days of these locations is depicted in figure 4.14c. The degradability data used was gathered in a study done earlier on these samples (Zander et al., 2020).

Location	Average		
	TOC %	mg C / g TOC degraded (250 days)	mg C / g TOC degraded (21 days)
SW	2,5	79	12
RV	6,2	115	27
RT	4,1	107	26
KH	3,8	74	15

Table 4.2: Average TOC %, mg C / g TOC after 250 days and mg C / g TOC after 21 days for the locations SW, RV, RT and KH.
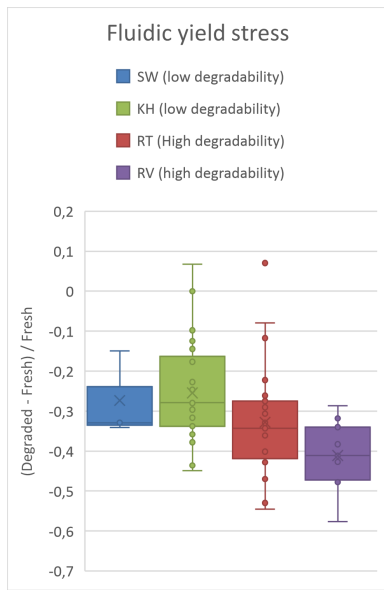
(a)
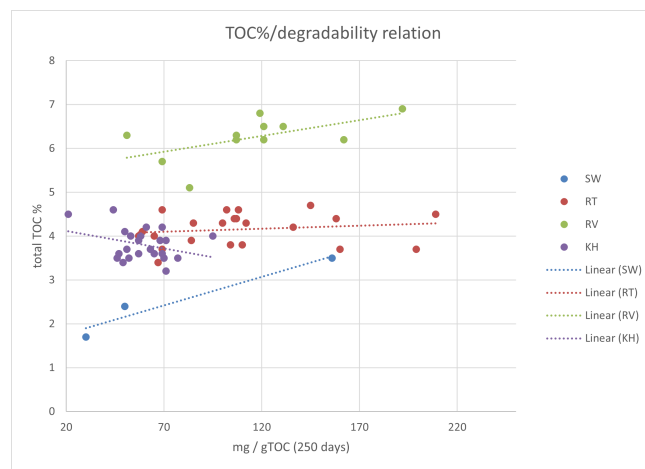
(b)
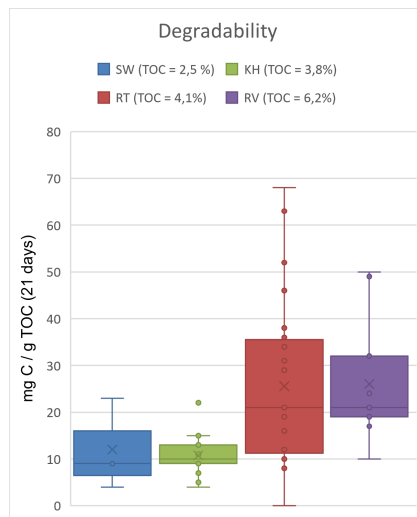
(c)

Figure 4.14: In (a), the relative fluidic yield stress differences are plotted for the locations SW, RV, RT and KH. In (b), the TOC percentages are given as a function of degradability after 250 days. In (c), a box plot for these locations of the degradability after 21 days is depicted.

(a)   (b)
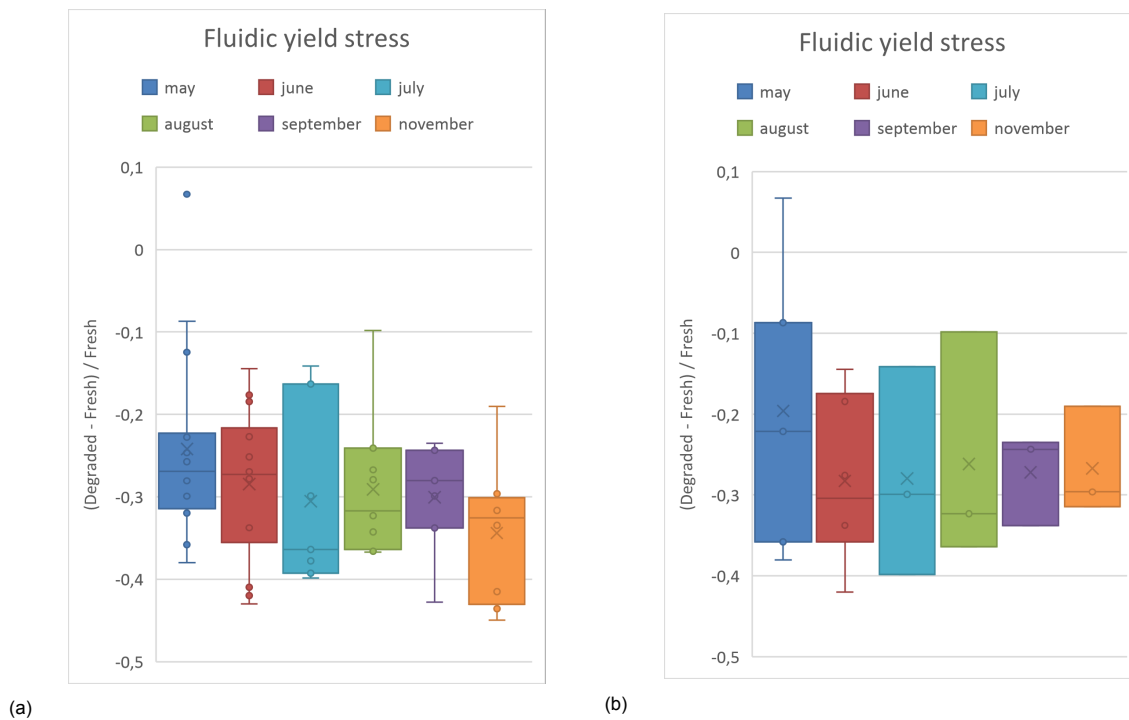
Figure 4.15: All τ_y^f of the anaerobically degraded sample minus their fresh counterparts, and then divided by the fresh results for locations KH, RT and RV (left). Onlys the PS samples (right). Sorted by sample season.

4.5.1. Discussion

As stated before, a positive correlation between TOC % and degradability makes linking this degradability with the relative yield stress changes difficult. This correlation is present because both the TOC % and degradability are dependent similarly on the positioning within the port; the TOC % and degradability are higher for more upstream locations. This is clearly visible when comparing table 4.2 with figure 3.1. For this reason, the influence of degradability and TOC % could not be distinguished from the data obtained in this research.

In figure 4.14c, the locations RT and RV do not show a clear difference. However, the degradability in the samples from locations SW and KH display remarkably little scatter. The lack of samples with a high degradability from location KH could be accredited to the hindered settling this location has seen in situ. KH is the only location that was regularly dredged with a water injection dredger. The carbon present in the sample could therefore have been in a different state than the other locations; less degradable. The lack of scattering for location SW can be ignored, as the location contains only 3 data points.

4.6. The seasonal variability

In this section, the seasonal variability on the degradation effect is investigated. This can be done by comparing the results from samples taken on different campaigns. However, as most locations were only visited on a few campaigns, this would not lead to a clear insight on the seasonal effect. For this reason the three locations with the most samples are selected: Köhlfleethafen (KH), Reiherstieg Vorhafen (RV) and Rethe (RT). The results for the fluidic yield stress from the six months in which the samples were taken are depicted in figure 4.15a. Furthermore, the other results are shown in figure E.8. No clear trend seems to be visible between the months. However, November clearly shows a more considerable decline in most characteristics.

4.6.1. Discussion

The decline in November is interesting as this is the only winter month in which samples have been taken. It is noticeable that the average density of the samples in November is lower than the rest of

Average impact fraction	Anaerobic degradation	Aerobic degradation
Static yield stress (τ_y^s)	-0.25	+0.05
Fluidic yield stress (τ_y^f)	-0.19	+0.02

Table 4.3: The average weighted τ_y^s and τ_y^f differences for the anaerobically and aerobically degradded samples.

the samples. This is due to the lack of samples in the FM layer this month. In figure E.10 the reported FM layer sizes of location KH have been plotted by date. The size of the FM layer is at a minimum in November. Furthermore, the FM samples in November showed a very high density compared to other FM samples. Additionally, the yield stresses for these samples are also of a magnitude most commonly observed at PS/FM or PS layers. This indicates that the November FM samples are actually more like PS/FM or even PS layers. It was noticed in section 4.3 that the degradation has more (absolute) effect on denser mud layers. The lack of the FM layer, and therefore FM samples, can thus explain the more significant decrease in November. Furthermore, the yield stresses from the FM samples from location KH are shown in figure E.11.

Box plots of only the PS samples of the same locations are made to test this explanation. The results for the τ_y^f are shown in figure 4.15b and the other parameters are displayed in figure E.9. The increased impact for November is not visible anymore, which confirms this explanation. The effect of the seasonality on the impact of the degradation on the rheology can therefore not be confirmed.

4.7. The effect of the availability of oxygen

For the last sub-question, aerobically degraded samples were tested. Only a little aerobically degraded sample was available (often just enough for one test, sometimes not enough), so only a stress sweep was performed on these samples. Therefore just the τ_y^s and τ_y^f were obtained, which are plotted next to the anaerobic results of the same samples in figure 4.16.

Clear differences are noticeable between the result. The average impact fractions (y-axis in graph 4.16) are shown in table 4.3. A clear dissimilarity exists between the samples; the anaerobically degraded samples show a clear reduction in strength, while the aerobically degraded samples do not.

4.7.1. Discussion

This significant difference between the two was unexpected as the degradation rates in aerobic conditions are known to be several times higher than in anaerobic conditions. Some other phenomenon seems to make up for this loss in strength.

One theory is the oxidation of ions within the sample once it comes into contact with oxygen. As the samples under examination came from the river and were thus preserved in anaerobic conditions, the ions were dissolved until the sample was taken. Once the sample came into contact with oxygen, the iron dissipated, and Fe oxides were formed. The oxidation of these ions could give additional strength to the structure, disguising the OM degradation effect. This theory is supported by the visual differences between anaerobically and aerobically incubated samples; anaerobically degraded samples have a dark colour, and the aerobically degraded samples have a more orange/brown colour. These colours are shown in figure E.12.

4.8. Structural recovery

The trends presented in this chapter have not been visible for the structural recovery fraction and structural recovery time (tr). The correlations of the rheological parameters with density, TOC % and degradability are not visible for G_∞'/G_0' because this is a fraction. Both the numerator and denominator are thus dependent on these influences. When the recovery fractions of the fresh samples are subtracted from the ones from the degraded samples, though, something is visible. In figure 4.17 the structural recovery fractions and t_r result for the PS layer of locations RT and KH are depicted. These locations were selected because they have sufficient samples from the PS layer to say something about the averages. The average (degraded - fresh) recovery fractions for RT and KH are above zero; 0,02 and 0,08 respectively.
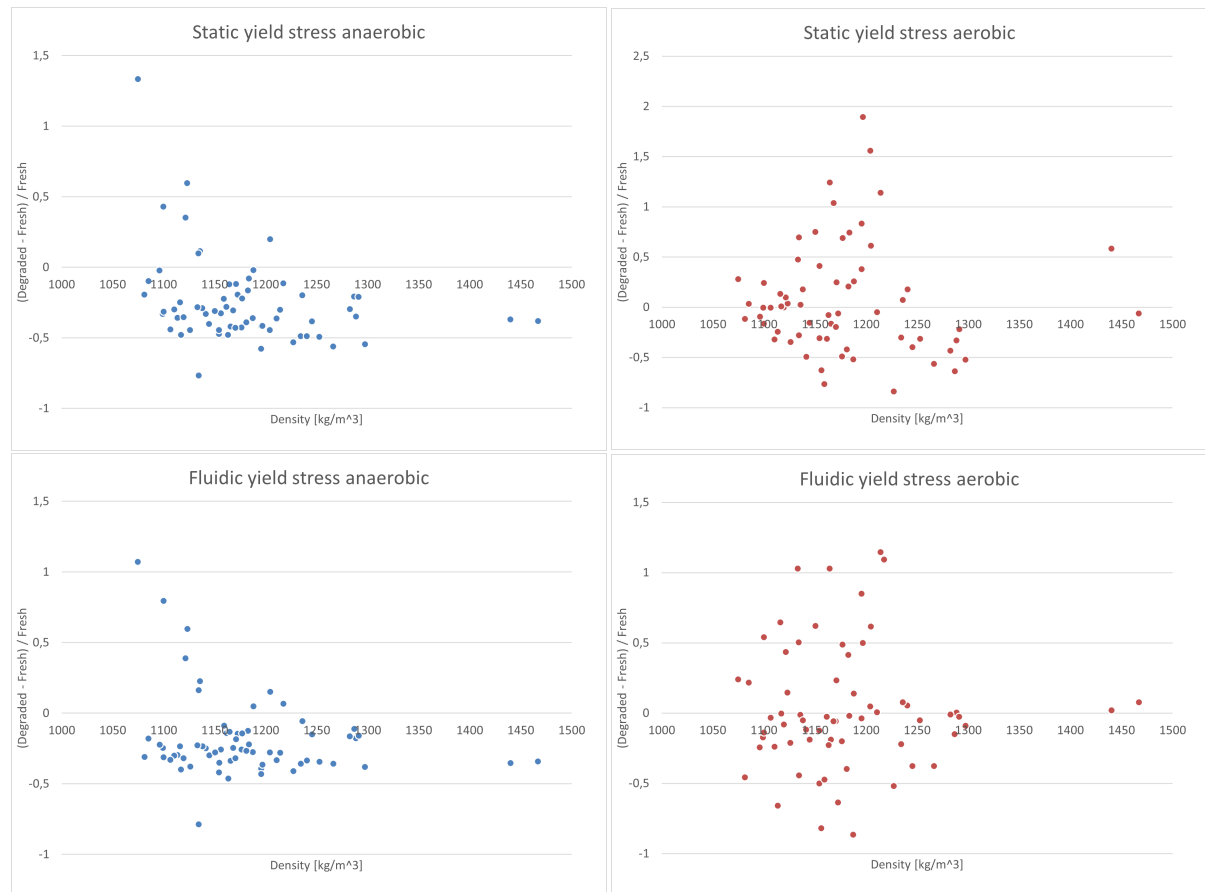
Figure 4.16: The yield stresses of the anaerobically and aerobically degraded samples as a function of the density.

The structural recovery fraction represents the strength of the sample still present after a period of shearing. As the OM partly provides this strength in the mud, and the shearing breaks up the structure caused by the OM, a decrease in OM due to degradation is expected to decrease the effect of shearing. The fraction of the degraded sample would then be higher, and therefore the results in figure 4.17a would be positive, which is indeed shown for locations RT and KH. The 63 % recovery time for the same samples shows similar results in figure 4.17b.

4.9. The influence of OM degradation on the density-yield stress correlation

In research done by A. Shakeel, the fluidic yield stress was plotted as a function of excess density (ρ-ρ_w = $\rho - 1000$), and the data were fitted using a power law. In this study, the fluidic yield stresses for the fresh and degraded mud samples for two locations are fitted with equation 4.1, which was adapted from the equation introduced by A. Shakeel (location RV was also plotted, but will be discussed in section 4.9.1)(Shakeel, A., et al., 2021). The results are depicted in figure **??**. These locations were chosen because they contain the largest number of samples.

$$\tau_f = a \cdot ((\rho - \rho_w)/\rho_w)^b \qquad (4.1)$$

In A. Shakeel's research, the fit for different locations showed similar values for fitting parameter 'b', while differing in fitting parameter 'a' (i.e. the slopes stay the same) (Shakeel, A., et al., 2021). In figure 4.18, the trends are also visible with similar values for 'b' while only the 'a' alters significantly
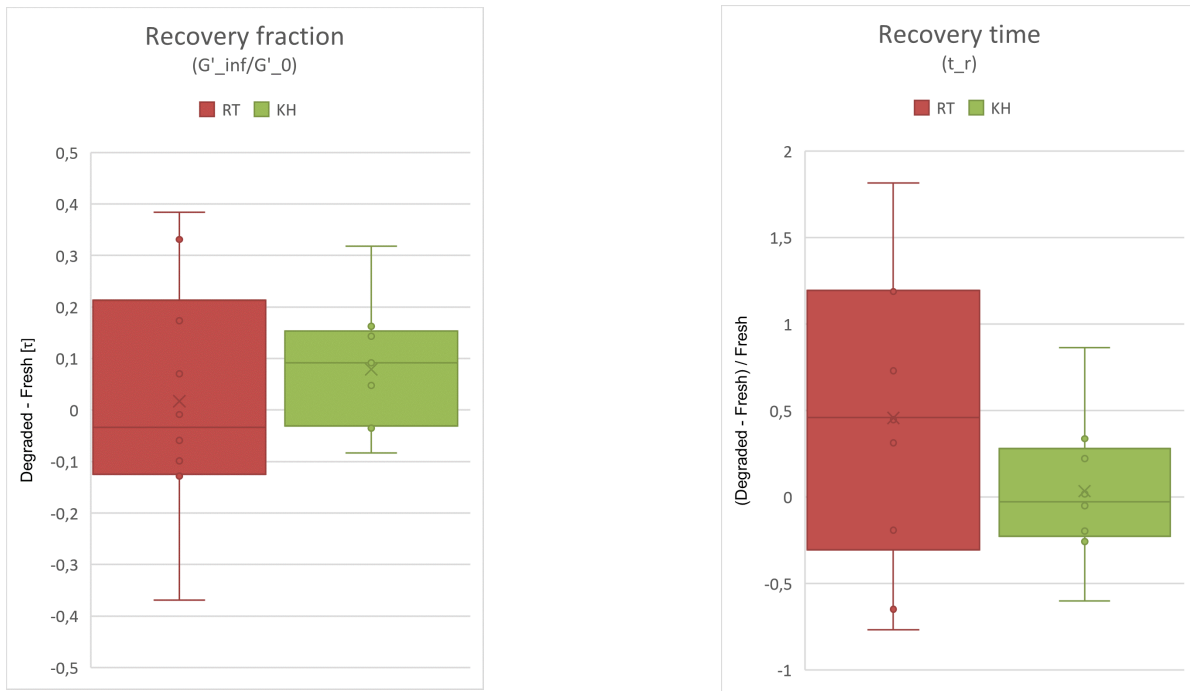
Figure 4.17: The structural recovery fractions and structural recovery time for the PS layer of RT and KH. The average recovery fraction and structural recovery time are 1,406 and 5619 respectively.

between the fresh and degraded samples. This result verifies that the correlation between density and yield stress is strongly affected by TOC content (either caused by spatial variation or OM degradation). However, it is interesting to note that the decrease in TOC content after degradation is about 4,5 to 16,5 % (for all locations), which is not very significant compared to the change in yield stresses. Therefore, another reason could be the structural breakdown of the OM or breakdown of organic bridges between OM and clay particles.

4.9.1. b-values

A sufficient amount of samples are needed for a reliable fitting of the data. In this study, only three locations were sampled frequently enough to obtain a good data fitting; KH, RT and RV. Though similar 'b-values' were obtained for KH and RT (around 3,8), the b-values of the fresh and degraded samples
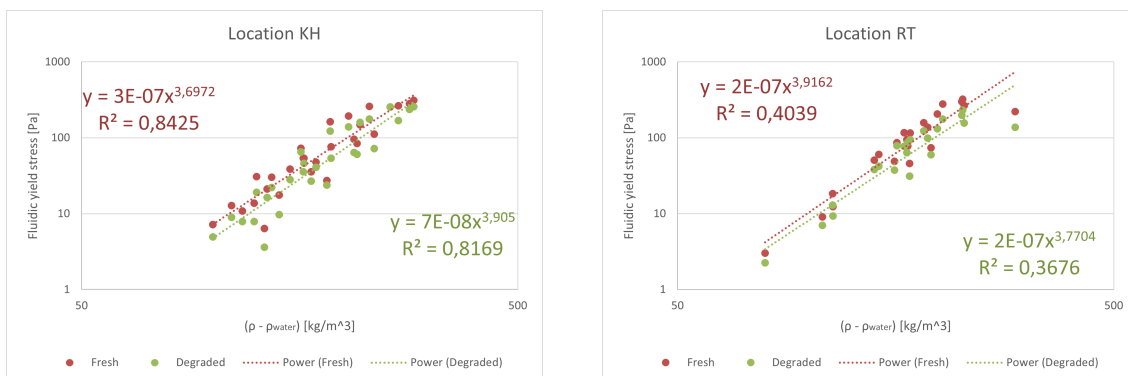
Figure 4.18: Fluidic yield stress as a function of exsess density $(\rho - \rho_w)$ for fresh and degraded mud samples from (a) location KH, (b) location RT. The dashed lines represent the power law fitting by using equation 4.1 and the parameters of the equation are shown on the graphs.

(a)   (b)

(c)
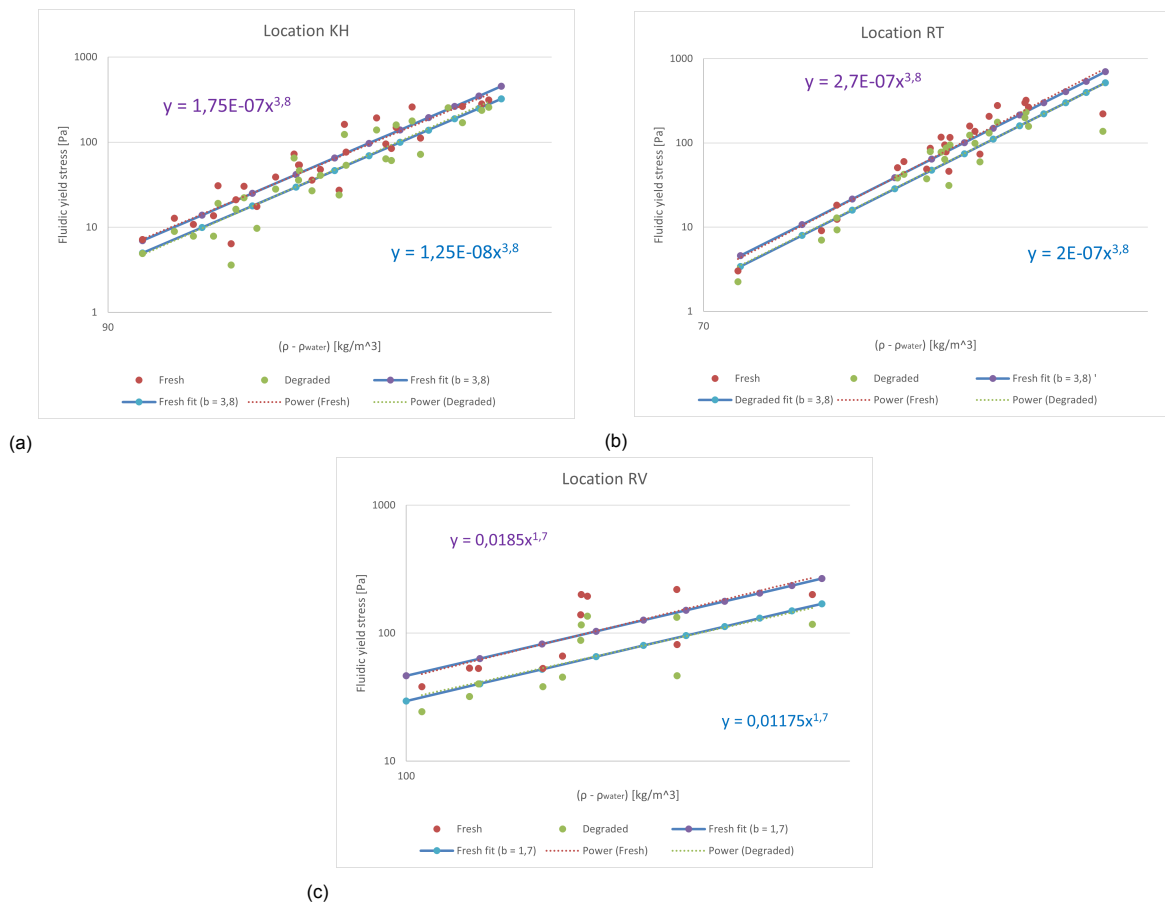
Figure 4.19: The fluidic yield stresses of the fresh and degraded samples for locations (a) KH, (b) RT and (c) RV. The red and green dashed lines represent the original fittings, with the equation and R^2 given. The purple and blue lines represent the secondary fitting, with identical b-values for the fresh and degraded samples.

of location RV were 1,789 and 1,619, respectively. RV is, therefore, clearly a particular case. With this in mind, the a-values were taken into consideration nevertheless.

The b-values for the fresh and anaerobically degraded samples are almost identical for all three locations. Therefore, the fresh and degraded samples were fitted again, with the same b-value for the fresh and degraded data sets. Locations KH, RT and RV were fitted with a b-value of 3.8, 3.8 and 1.7 respectively as depicted in figure 4.19.

4.9.2. a-values

In figure 4.20, the a-values obtained with the fitting in figure 4.19 are plotted as a function of (a) the average TOC (mass)percentages and (b) the average mg C / g TOC emitted after 250 days of the samples from which the a-values were derived. From figure 4.20a, it can be deduced that the a-values do not depend much on mg C / g TOC after 250 days, as these values vary significantly between locations KH an RT; 73,7 and 107 respectively. For a similar degradability (114,8 mg C / g TOC), a very high a-value is found for location RV; the degradability seems to have a huge influence here. Combined with the deviating b-value, this makes RV a particular case.

In figure 4.20b, the a-values are given as a function of the average TOC % of the samples. Here, a trend can be observed; the a-values seem to be positively correlated with the TOC %. If the trend is linear, the angle would be given by equation 4.2, where α represents the slope of the trend. Consequently, a figure plotting α (= a-value / TOC %) as a function of average fluidic yield stress should then result in a horizontal line. However, as shown in figure 4.20c, this is not precisely correct. This was also found by A. Shakeel (figure 9d in the article)(Shakeel, A., et al., 2021).

(a)

(b)

(c)
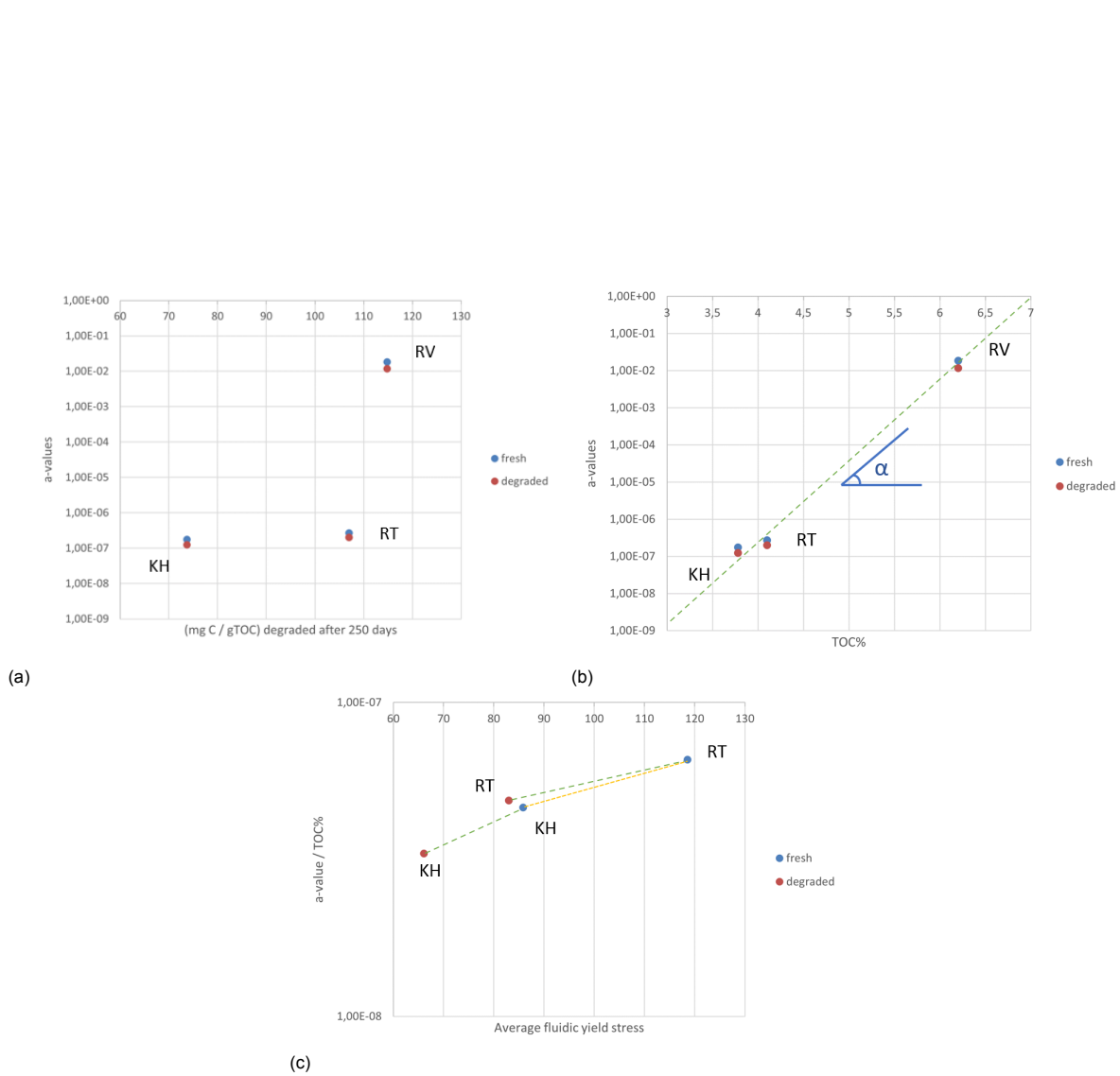
Figure 4.20: The a-values derived from figure 4.19 as a function of the average (a) the average TOC (mass)percentages and (b) the average mg C / g TOC emitted after 250 days of the samples from which the a-values were derived. In figure (c), the a-values of location RT and KH are divided with the TOC % and plotted as a function of the average fluidic yield stress of the samples.

$$a - value = \alpha * TOC\% \qquad (4.2)$$

4.9.3. Alpha

α seems to decrease with degradation. This would imply that α is a function of degradation, and can therefore be estimated by equation 4.3a, with slope α' given by equation 4.3b. Here, α_f and α_d represent the alpha values for the fresh and degraded samples, respectively.

Then, knowing that $\alpha = \alpha_f$ when mgC / gTOC = 0 and and $\alpha = \alpha_d$ when mgC / gTOC after 250 days (i.e. fully degraded after 250 days), this results in equation 4.4. Here, α_f could be constant for each location. This would mean if the TOC changes at a location, the a-value$_{fresh}$ changes with TOC according to $a - value_{fresh} = TOC\% * \alpha_f$. However, from the samples examined in this research this could not be verified sufficiently.

$$\alpha = \alpha_f - \alpha' * \frac{mgC}{gTOC} \qquad (4.3a)$$

$$\alpha' = \frac{\alpha_f - \alpha_d}{\frac{mgC}{gTOC}} \qquad (4.3b)$$

$$a - value = TOC\% * (\alpha_f - \alpha' * mgC/gTOC) \qquad (4.4)$$

Finally, equation 4.1 and 4.4 can be combined into equation 4.5. This formula is a proposition for the dependence of the fluidic yield stress (τ_f) as a function of density, TOC % and degradability. This equation is only useful if α_f and α' are constant for each location (i.e. independent of TOC%). However, the difference between the fresh a-values in figure 4.20c (the yellow line) indicates α_f cannot be generalised for all locations. One reason for this is that the 'fresh' samples considered were taken from situ and are thus already partially degraded when the measurements start. These amounts of already degraded OM vary per location, which is not considered in equation 4.5.

$$\tau_f = TOC\% * (\alpha_f - \alpha' * \frac{mgC}{gTOC}) * (\frac{\rho - \rho_{water}}{\rho_{water}})^b \qquad (4.5)$$

5

Conclusions

Developing improved sediment management techniques requires a clear understanding of the rheological properties of natural mud. These properties are greatly dependent on several parameters. Particularly the organic matter content of the mud. However, this organic matter will degrade over time, and this process is therefore expected to affect the rheological properties of the mud. Samples from different depths and locations (to vary the TOC content and density) of the port of Hamburg were studied to analyse this hypothesis. The rheological properties of the fresh and degraded samples were then compared in this study. The key findings of this research will be set out by firstly answering the sub-questions below, and after that, a conclusion is drawn based on the main research question and research objective.

- 1. Does the effect of organic matter degradation on the rheology of mud differ for different densities?
Anaerobic degradation clearly affects the rheological properties of the samples. After degradation, the degraded samples' strength (yield stresses) are a certain percentage of their original strength. After 250 days of degradation, the average strength left is 74% of the original strength (average for all locations and densities). It was found that the effect of density could be decoupled from the effect of OM degradation and TOC: for all samples (except for location RT), degraded or fresh, the dependence on density is of the form $((\rho - \rho_{water})/\rho_{water})^{3,8}$.
The hypothesis "the rheological properties of a denser layer of mud are less affected by OM degradation than those of a less dense layer" is confirmed, as the absolute differences are larger with denser samples.

- 2. What is the effect of different amounts of organic matter on the rheology of mud before and after degradation?
The data gathered in this study shows a clear dependency of the decline in strength due to OM degradation on the TOC % present in the sample. The τ_y^s, τ_y^f, cross-over amplitudes, G^* and hysteresis loop surfaces decline more for samples with a higher TOC %. The relative differences in yield stresses are not depending on TOC % for $\rho < 1200$ [kg/m^3]. For $1200 < \rho$ [kg/m^3], a dependence on TOC % is found. The hypothesis "the rheology of mud with a relatively large amount of OM will be affected more by degradation than the rheology of mud with a relatively small amount of OM" has thus been confirmed.

- 3. What is the effect of the degradability of the organic matter on the rheology of natural mud?
The samples with higher degradability and TOC % (from a more upstream location) seem to be more affected than those with lower degradability and TOC % (from a more downstream location). The influence of degradability and TOC % could therefore not be distinguished. The results hint at a degradability-yield stress dependency when investigating the influence of OM degradation on the density-yield stress correlation. However, this could not be concluded definitively with the samples examined

41

in this research. For these reasons, the hypothesis "the rheological properties of an (otherwise similar) mud layer with a higher degradability are more affected than a sample with a lower degradability" could not be confirmed.

- 4. Is there any seasonal variability on the effect of organic matter degradation on the rheology of mud?

The effects of degradation on the rheology of the mud samples do not vary significantly between samples taken in different months. Therefore, the hypothesis "the effect of OM degradation on the rheological properties of mud is not affected by seasonal changes" is confirmed.

- 5. Does the effect of organic matter degradation on the rheology of mud differ for aerobic and anaerobic conditions?

The anaerobically degraded samples' average static and fluidic yield stress decreased by 25 and 19 %, respectively. However, the aerobically degraded samples increased with a respective 5 and 2 %. The additional strength is suspected of coming from oxidised ions. Therefore, the hypothesis "the aerobic degradation has a more significant impact on the rheological properties of mud than anaerobic degradation" has been disproven.

With the sub-questions answered, an answer can be formulated to the main research question; "What are the effects of organic matter degradation on the rheological properties of natural mud?"
There is a big scatter in the strength of aerobically degraded mud, while 250 days of anaerobic degradation has a significant (20 - 30 %) impact on most rheological properties. Though the absolute strength of the fresh mud is primarily dependent on density and TOC %, the percentage primarily correlates with the TOC % and the degradability of this organic matter.

Lastly, it can be assessed whether the research objective has been achieved; "Clearing the path to improved sediment management techniques by quantifying one unknown variable; the effect of organic matter degradation on the rheology of mud."
With a large amount of data, some clear density-, TOC %- and degradability-dependent trends were identified and presented. These trends can function as a first indication as to the scale and precise implications of the degradation effect. This study, therefore, contributes to a better understanding of the versatile rheology of mud. Intentional degradation by dredging operations could prove to be very effective in making the mud navigable. Though oxidation of the mud should be handled with care, as ion formation could strengthen the mud.

6

Recommendations

The presented discussions and conclusions considered, some recommendations for future research are given in this chapter. Some tips for conducting a similar experimental study will be given. Additionally, a few interesting follow-up research subjects will be recommended.

- First of all, for this research, many locations (11) were used to acquire samples for this research. When processing the data, though, this complicates analysing the results. As only a few data points were available for many locations (and these locations differ in things like TOC % and degradability), the amount of data that could be used to investigate specific influences on the rheological parameters was limited. Therefore, it is recommended that more samples from the same locations be analysed in future research.

- Because of the low density, the rheological parameters of many samples from the FM layer could not be measured sufficiently precisely from the data obtained from the rheometer. This has led to a limited number of data points for this layer throughout this study. This is unfortunate as the FM layer is the most exciting. Indeed, it is the rheological property of the FM layer that determines whether this layer is navigable or not. Therefore, more samples from the FM layer would be an excellent addition to this study, as this surplus would make up for the data lost by the failed experiments.

- Furthermore, though the samples of this research could be grouped into categories (same density, same layer...), they still differed for their other variables. Further studies are required to look into the specific influences of each parameter on rheology. Therefore, this could add more precision to any model predicting the influence of OM degradation on the density-yield stress correlation. For example, rheological tests done on samples of known composition (containing organic matter of known type, concentration and state of degradation) would confirm the hypothesis made regarding the relations between TOC and degradability.

- All samples examined in this research have been degraded for 250 days. Comparing these results with the results obtained from samples degraded for a longer or shorter period would be interesting. As the degradation happens gradually over time, a better understanding of the timescales related to degradation will be obtained.

- The influence of different sand contents on the rheology of mud would be another exciting subject for further research. Segregation of sand and mud is an interesting topic in itself, but this research will also be of value for specific areas of ports. The rheological behaviour of mud upon degradation of organic matter could differ in sand-rich areas as compared to clay-rich areas.

- The scatter of the aerobically degraded samples data in this study are likely to be caused by oxidising ions. However, these samples have been in contact with more oxygen than a fluid mud layer would. Therefore, a closer look into the rheology of mud at different oxygen levels available would be interesting.

Appendices

A
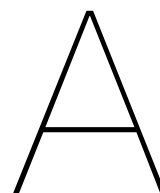
Halfreactions

Compound	Half reaction	$\Delta G_r^0 \left(\text{kJ} \, (\text{e}^-)^{-1} \right) 25°C$
TEA reaction		
Oxygen	$O_2 + 4e^- + 4H^+ \rightarrow 2H_2O$	-122.7
Nitrate	$NO_3^- + 5e^- + 6H^+ \rightarrow 1/2 \, N_2 + 3H_2O$	-118.3
Pyrolusite	$MnO_2 + 4H^+ + 2e^- \rightarrow Mn^{2+} + 2H_2O$	-120.0
Goethite	$FeOOH + 3 \, H^+ + e^- \rightarrow Fe^{2+} + 2H_2O$	-75.9
Hematite	$Fe_2O_3 + 6H^+ + 2e^- \rightarrow 2Fe^{2+} + 3H_2O$	-74.6
2-line Ferrigydrite	$Fe(OH)_3 + 3H^+ + e^- \rightarrow Fe^{2+} + 3H_2O$	-94.7
Sulfate	$SO_4^{2-} + 8e^- + 9H^+ \rightarrow HS^- + 4H_2O$	-24.0
Electron donor (ED) reaction		
Amino acids		
Serine	$C_3H_7NO_3 + 6H_2O \leftrightarrow 3HCO_3^- + 13H^+ + NH_4^+ + 10e^-$	10.18
Asparagine	$C_4H_8 \, N_2O_3 + 9H_2O \leftrightarrow 4HCO_3^- + 14H^+ + 2NH_4^+ + 12e^-$	12.82
Alanine	$C_3H_7NO_2 + 7H_2O \leftrightarrow 3HCO_3^- + 14H^+ + NH_4^+ + 12e^-$	16.00
Tryptophan	$C_{11}H_{12} \, N_2O_2 + 31H_2O \leftrightarrow 11HCO_3^- + 55H^+ + 2NH_4^+ + 46e^-$	18.49
Mononucleotides		
Adenosine-MP	$C_{10}H_{12} \, N_5O_7P^{2-} + 27H_2O \leftrightarrow 10HCO_3^- + 35H^+ + 5NH_4^+ + 30e^- + HPO_4^{2-}$	2.85
Deoxycytidine	$C_9H_{12} \, N_3O_7P^{2-} + 24H_2O \leftrightarrow 9HCO_3^- + 38H^+ + 3NH_4^+ + 32e^- + HPO_4^{2-}$	10.23
Saccharides		
Glucose	$C_6H_{12}O_6 + 12H_2O \rightarrow 6HCO_3^- + 24e^- + 30H^+$	10.0
Deoxyribose	$C_5H_{10}O_4 + 11H_2O \mapsto 5HCO_3^- + 22e^- + 27H^+$	12.66
Membrane-type compounds		
C_{16} n-alkane	$C_{16}H_{34} + 48H_2O \leftrightarrow 16HCO_3^- + 114H^+ + 98e^-$	19.84
Hopane	$C_{30}H_{52} + 90H_2O \leftrightarrow 30HCO_3^- + 202H^+ + 172e^-$	20.61
Complex organics		
Type I kerogen	$C_{415}H_{698}O_{22} + 1223H_2O \leftrightarrow 2729H^+ + 415HCO_3^- + 2314e^-$	19.95
Fulvic substance	$C_{27}H_{28}O_7 + 74H_2O \leftrightarrow 149H^+ + 27HCO_3^- + 122e^-$	20.73
Misc species		
Hydrogen	$H_2 \rightarrow 2H^+ + 2e^-$	-8.9
Formate	$CHO_2^- + H_2O \leftrightarrow 2H^+ + HCO_3^- + 2e^-$	0.56
Ammonia	$NH_3 \rightarrow 1/2 \, N_2 + 3e^- + 3H^+$	11.9
Acetate	$C_2H_3O_2^- + 4H_2O \leftrightarrow 9H^+ + 2HCO_3^- + 8e^-$	18.02
Methane	$CH_4 + 3H_2O \rightarrow 9H^+ + HCO_3^- + 8e^-$	19.9
Hydrogen sulfide	$HS^- + 4H_2O \rightarrow SO_4^{2-} + 8e^- + 9H^+$	24.0
Ferrous Iron	$Fe^{2+} \rightarrow e^- + Fe^{3+}$	74.2

Table A.1: Half-reactions of common terminal electron acceptors (TEAs) and electron donors (EDs). Taken from Arndt et al., 2013.

B

Geometry

In a rotational rheometer the shear stress τ is given by equation B.1, the strain γ by equation B.2 and the shear rate (or strain-rate) $\dot{\gamma}$ by equation B.3. Where M_d is the torque applied (or measured), ϕ is the angle and Ω the angular velocity applied (or measured). A and M are geometry factors which are, for a Couette geometry like figure 3.3b, given by equation B.4 and B.6 respectively. Furthermore, radius ratio δ is defined as equation B.5, the viscosity is defined as equation B.7, and C_L equals 1,1 (*HAAKE MARS Rheometer Instruction Manual*, 2014). The values for these parameters for the geometry used in this research can be found in table B.1.

$$\tau = AM_d \tag{B.1}$$

$$\gamma = M\phi \tag{B.2}$$

$$\dot{\gamma} = M\Omega \tag{B.3}$$

$$A = \frac{1}{2\pi R_i^2 L C_L} \frac{1 + \delta^2}{2\delta^2} \tag{B.4}$$

$$\delta = \frac{R_a}{R_i} \tag{B.5}$$

$$M = \frac{1 + \delta^2}{\delta^2 - 1} \tag{B.6}$$

$$\eta = \frac{\tau}{\dot{\gamma}} \tag{B.7}$$

Parameter	Value for CC25 DIN Ti
R_i (mm)	12.54
L (mm)	37.6
Inertia I (kg m^{2} 10^{-6})	4.35
Mass m (g)	64.2
Geometry factor A [Pa/Nm]	22630
Geometry factor M [$fracs^{-1}rad^{-1}$]	12.35
Radius ratio δ	1.0845
Material	Titanium 3.7035

Table B.1: Parameters for the Couette CC25 DIN Ti geometry, taken from *HAAKE MARS Rheometer Instruction Manual*, 2014.

C

Matlab files

```
%                          Amplitude Sweep
clear all; close all; clc;
                              % Fresh sample
%Read all G' and tau from the first Excel file
sr_0 = readtable('ASweep_1Hz.xlsx','sheet', "ASweep_1Hz_rwd",'Range','D1:D500');
tau_0=sr_0.x_InN_m_;
ss_0 = readtable('ASweep_1Hz.xlsx','sheet', "ASweep_1Hz_rwd",'Range','F1:F500');
Gp_0=ss_0.G_InPa;


%Read all G" and tau from the first Excel file
sr_1 = readtable('ASweep_1Hz.xlsx','sheet', "ASweep_1Hz_rwd",'Range','D1:D500');
tau_1=sr_1.x_InN_m_;
ss_1 = readtable('ASweep_1Hz.xlsx','sheet', "ASweep_1Hz_rwd",'Range','G1:G500');
Gdp_1=ss_1.G_InPa;



                              % Degraded sample
%Read all G' and tau from the second Excel file
sr_2 = readtable('ASweep_1Hz.xlsx','sheet', "ASweep_1Hz_degraded_rwd",'Range','D1:D500');
tau_2=sr_2.x_InN_m_;
ss_2 = readtable('ASweep_1Hz.xlsx','sheet', "ASweep_1Hz_degraded_rwd",'Range','F1:F500');
Gp_2=ss_2.G_InPa;

%Read all G" and tau from the second Excel file
sr_3 = readtable('ASweep_1Hz.xlsx','sheet', "ASweep_1Hz_degraded_rwd",'Range','D1:D500');
tau_3=sr_3.x_InN_m_;
ss_3 = readtable('ASweep_1Hz.xlsx','sheet', "ASweep_1Hz_degraded_rwd",'Range','G1:G500');
Gdp_3=ss_3.G_InPa;
```

(a) part 1

```
LG1f=[transpose(tau_0);transpose(Gp_0)]; %Form vectors for the first excel file
LG2f=[transpose(tau_1);transpose(Gdp_1)];
P_fresh = InterX(LG1f,LG2f);              %Search for the crossings using function interX.m
P_fresh([2],:) = [];                      %Take the Amplitudes from the crossings, forget the moduli
CROSS_AMPLITUDE_fresh = max(P_fresh);     %Select the highest (the lowest is often a error caused by small data)
disp(CROSS_AMPLITUDE_fresh)               %Print the cross-over amplitude

LG1d=[transpose(tau_2);transpose(Gp_2)];
LG2d=[transpose(tau_3);transpose(Gdp_3)];
P_degraded = InterX(LG1d,LG2d);           %Same for the second ecxel file
P_degraded([2],:) = [];
CROSS_AMPLITUDE_degraded = max(P_degraded);
disp(CROSS_AMPLITUDE_degraded)


figure
semilogy(tau_0,Gp_0,'k-+'); hold on       %Display the graph
semilogy(tau_1,Gdp_1,'k-o'); hold on
semilogy(tau_2,Gp_2,'r-+'); hold on
semilogy(tau_3,Gdp_3,'r-o')
grid on
ylabel('Moduli [Pa]')
xlabel('Amplitude [Pa]')
title('Amplitude Sweep')
legend('Fresh G''','Fresh G"','Degraded G''', 'Degraded G"', 'Crossover stress' ,'location', 'Southwest')
```

(b) part 2

Figure C.1: The Matlab code used for retrieving the cross over amplitude from the frequency sweep data.

```
%                                  Thixotropic loop
clear all; close all; clc;

%                                  Fresh sample
%Read the Excel and make a vector that canbe used by interX.m
sr_0 = readtable('CSRT.xlsx','sheet', "CSRT_rwd",'Range','B1:B55');      %with my settings 55 was the turning point
g_d_0=sr_0.x__In1_s;                                                     %so that could differ
ss_0 = readtable('CSRT.xlsx','sheet', "CSRT_rwd",'Range','C1:C55');
tau_0=ss_0.x_InN_m_;
freshxheen = transpose(g_d_0);
freshyheen = transpose(tau_0);
freshheen = [freshxheen;freshyheen]

%    Make the vector after shearing for interX.m
sr_1 = readtable('CSRT.xlsx','sheet', "CSRT_rwd",'Range','B55:B106');    %Alter the numerbers to your data
g_d_1= table2array(sr_1);
ss_1 = readtable('CSRT.xlsx','sheet', "CSRT_rwd",'Range','C55:C106');
tau_1= table2array(ss_1);
freshxterug = transpose(g_d_1);
freshyterug = transpose(tau_1);
freshterug = [freshxterug;freshyterug];

PCSRT = InterX(freshheen,freshterug)     %Find the itersection
PCSRTmax = max(PCSRT)
PCSRTgood = max(PCSRTmax)

freshyheengoed = zeros(1,54);       %Set every y value before the intersection to zero
for c = 1:54
    if freshyheen(1,c) > PCSRTgood
        freshyheengoed(1,c) = freshyheen(1,c);
    else
        freshyheengoed(1,c) = 0;
    end
end
```

(a) part 1

```
%Take the surface below
gral1 = cumtrapz(freshxheen,freshyheengoed);
opp1 = gral1(1,54);

%Set every y value before the intersection to zero
freshyteruggoed = zeros(1,51);
for c = 1:51
    if freshyterug(1,c) > PCSRTgood
        freshyteruggoed(1,c) = freshyterug(1,c);
    else
        freshyteruggoed(1,c) = 0;
    end
end

%Take the surface below
gral2 = cumtrapz(freshxterug,freshyteruggoed);
opp2 = gral2(1,51);

%Determine and display the surface for the loop
SURFACE_CSRT_FRESH = opp1+opp2
disp(SURFACE_CSRT_FRESH)

%Plot the loop for visual reference
figure
plot(g_d_0,tau_0,'k-*'); hold on
plot(g_d_1,tau_1,'r-*')
grid on
ylabel('Stress [Pa]')
xlabel('Shear rate [s^{-1}]')
title('Thix. loop Fresh')
legend('Ramp up','Ramp down', 'location', 'Northwest')
```

(b) part 2

Figure C.2: The Matlab code used for retrieving the hysteresis loop surface from the thixotropic loop test data (first two parts).

```matlab
%                    Exactly the same for the second sample (in the same Excel file)
sr_0 = readtable('CSRT.xlsx','sheet', "CSRT_degraded_rwd",'Range','B1:B55');
g_d_0=sr_0.x__In1_s;
ss_0 = readtable('CSRT.xlsx','sheet', "CSRT_degraded_rwd",'Range','C1:C55');
tau_0=ss_0.x_InN_m_;

freshxheen = transpose(g_d_0);
freshyheen = transpose(tau_0);
freshheen = [freshxheen;freshyheen];

sr_1 = readtable('CSRT.xlsx','sheet', "CSRT_degraded_rwd",'Range','B55:B106');
g_d_1= table2array(sr_1);
ss_1 = readtable('CSRT.xlsx','sheet', "CSRT_degraded_rwd",'Range','C55:C106');
tau_1= table2array(ss_1);

freshxterug = transpose(g_d_1);
freshyterug = transpose(tau_1);
freshterug = [freshxterug;freshyterug];
PCSRT = InterX(freshheen,freshterug);
PCSRTmax = max(PCSRT);
PCSRTgood = max(PCSRTmax);
freshyheengoed = zeros(1,54);
for c = 1:54
    if freshyheen(1,c) > PCSRTgood
        freshyheengoed(1,c) = freshyheen(1,c);
    else
        freshyheengoed(1,c) = 0;
    end
end
```

(a) part 3

```matlab
gral1 = cumtrapz(freshxheen,freshyheengoed);
opp1 = gral1(1,54);
freshyteruggoed = zeros(1,51);

for c = 1:51
    if freshyterug(1,c) > PCSRTgood
        freshyteruggoed(1,c) = freshyterug(1,c);
    else
        freshyteruggoed(1,c) = 0;
    end
end

gral2 = cumtrapz(freshxterug,freshyteruggoed);
opp2 = gral2(1,51);
SURFACE_CSRT_DEGRADED = opp1+opp2
disp(SURFACE_CSRT_DEGRADED)

figure
plot(g_d_0,tau_0,'k-*'); hold on
plot(g_d_1,tau_1,'r-*')
grid on
ylabel('Stress [Pa]')
xlabel('Shear rate [s^{-1}]')
title('Thix. loop Degraded')
legend('Ramp up','Ramp down', 'location', 'Northwest')
```

(b) part 4

Figure C.3: The Matlab code used for retrieving the hysteresis loop surface from the thixotropic loop test data (last two parts).

```
%                                    Structural recovery
clear all; close all; clc

% Determine Gprime_zero (allways the biggest Gprime from the first part of the experiment)
dati = xlsread('Thix_recovery.xlsx', "Thix_recovery_rwd", 'D1:D100');
C1 = dati(:,1);
Gpzero = max(C1);

% Determine Gprime_i (allways the smallest Gprime from the last part of the experiment
dato = xlsread('Thix_recovery.xlsx', "Thix_recovery_rwd", 'D500:D750');
C2 = dato(:,1);
Gpi = min(C2);

% Devide the Gprimes from the recovery by Gprime_zero
data = dato/Gpzero;

% Read the time
time = xlsread('Thix_recovery.xlsx', "Thix_recovery_rwd", 'C533:C750');

% Define the fit options
x = time;
y = data;
s = fitoptions('Method','NonlinearLeastSquares',...
               'Lower',[0,0,1],...
               'Upper',[Inf,Inf,Inf],...
               'Startpoint',[0, 0, 100]);

% Fit a line over the Gprime/Gprime_zero data in the known function.
f = fittype('(a/b)+(((c-a)/b)*(1-exp(-(x/e)^d)))', 'problem', {'a', 'b'} , 'options', s);
[c1,gof1] = fit(x,y,f,'problem',{Gpi, Gpzero});      % set which parameters to find (Ginf_delta, tr)
huppeldepub = coeffvalues(c1);                       % make a vector from the found parameters
Ginf_f = huppeldepub(1,1)                            % display them
d_f = huppeldepub(1,2)
tr_f = huppeldepub(1,3)
```

(a) part 1

```
time1=time;data1=data; %change the name so one can write over it

%                Do the exact same thing for the second (degraded) sample data.
datid = xlsread('Thix_recovery.xlsx', "Thix_recovery_Degraded_rwd", 'D1:D100');
C1_d = datid(:,1);
Gpzero = max(C1_d);

datod = xlsread('Thix_recovery.xlsx', "Thix_recovery_Degraded_rwd", 'D500:D750');
C2_d = datod(:,1);
Gpi = min(C2_d);

data = datod/Gpzero;
time = xlsread('Thix_recovery.xlsx', "Thix_recovery_Degraded_rwd", 'C534:C750');
x = time; y = data;

[c2,gof2] = fit(x,y,f,'problem',{Gpi, Gpzero});
huppeldepub = coeffvalues(c2);
Ginf_d = huppeldepub(1,1)
d_d = huppeldepub(1,2)
tr_d = huppeldepub(1,3)

%    Plot both the data and the fitted curve over the data
figure
plot(time1,data1,'k*'); hold on
plot(c1, 'b'); hold on
plot(time,data,'r*'); hold on
plot(c2, 'g')
grid on
ylabel('Gp/Gpzero')
xlabel('time [s]')
title('Structural recovery')
legend('fresh','freshfit', 'Degraded', 'Degradedfit', 'location' ,'northeast')
```

(b) part 2

Figure C.4: The Matlab code used for retrieving .... from the structural recovery test data.

D
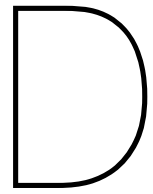
Data

The data obtained and used in this research is available through the TU Delft research data repository. It is also available upon request via C.Chassagne@tudelft.nl.

E
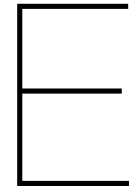
Additional tables and plots

Location	Coordinates (WGS 84)	
	degree N	degree E
Köhlbrand	53.529945	9.9385885
Rethe	53.511615	9.949098
Reiherstieg Vorhafen	53.477625	9.984925
Köhlfleet mit Köhlfleethafen	53.538894	9.991215
Sedimentfang Wedel	53.567833	9.679490
Parkhafen	53.533910	9.905856
Oortkaten	53.447645	10.096688
Dove Elbe	53.505052	10.060279
Zollenspieker	53.398950	10.186919
Lühesand	53.602375	9.584595
Au(ringels)eneste	53.543832	9.794888

Table E.1: The coordinates of the location from which samples have been examined in this study.
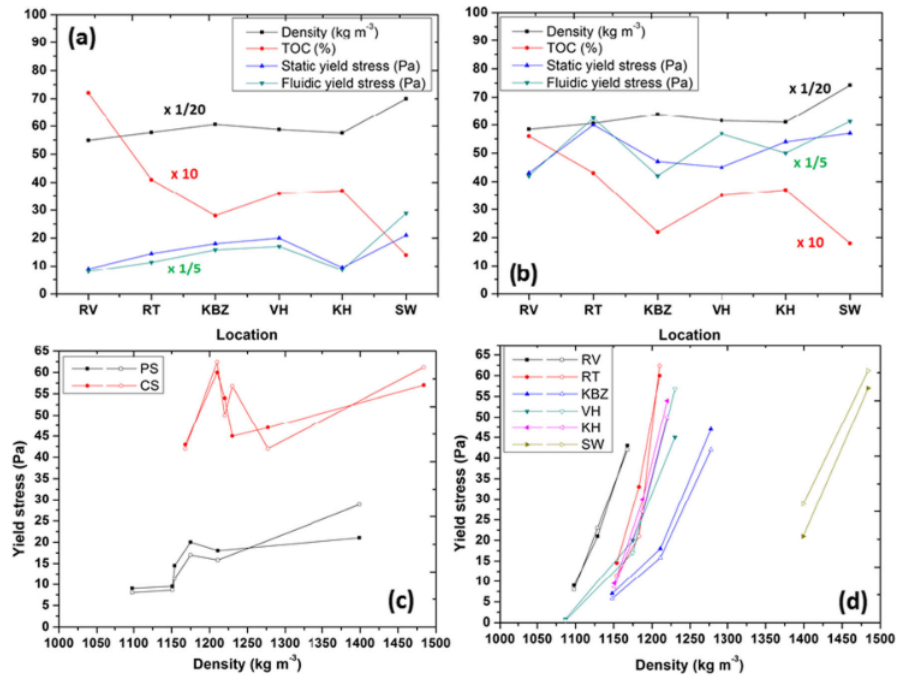
Figure E.1: The evolution of density, TOC, static- and fluidic yield stresses for different locations from the port of Hamburg. Figure a and b represent the PS and CS layer respectively. Filled symbols represent the static yield stresses and empty symbols represent fluidic yield stress values. Taken from Shakeel et al., 2020c.
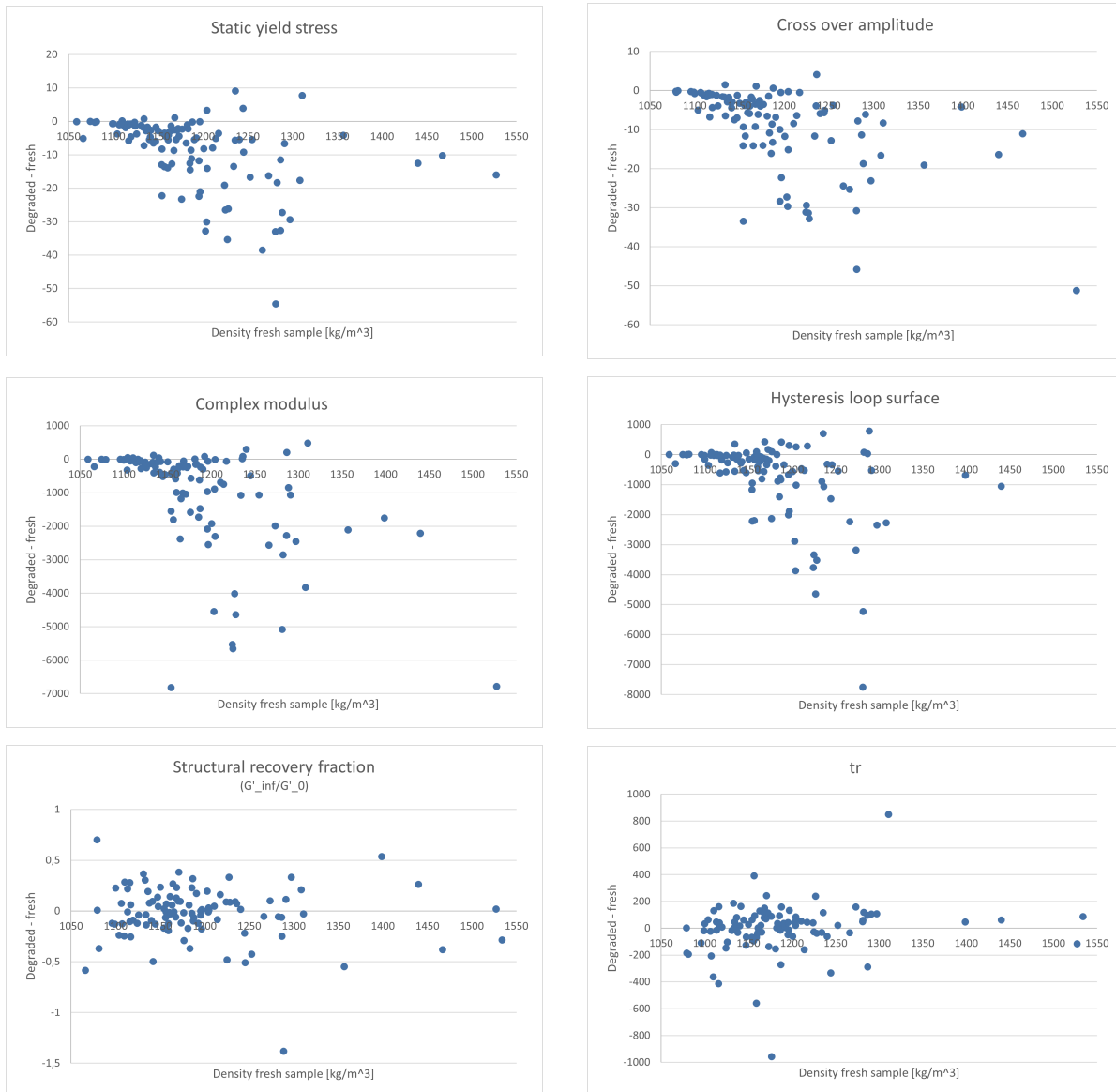
Figure E.2: The τ_y^s, cross-over amplitudes, G^*, hysteresis loop surfaces, G_∞'/G_0' and tr of the anaerobically degraded samples minus their fresh counterparts plotted as a function of the density of the fresh samples for all locations.
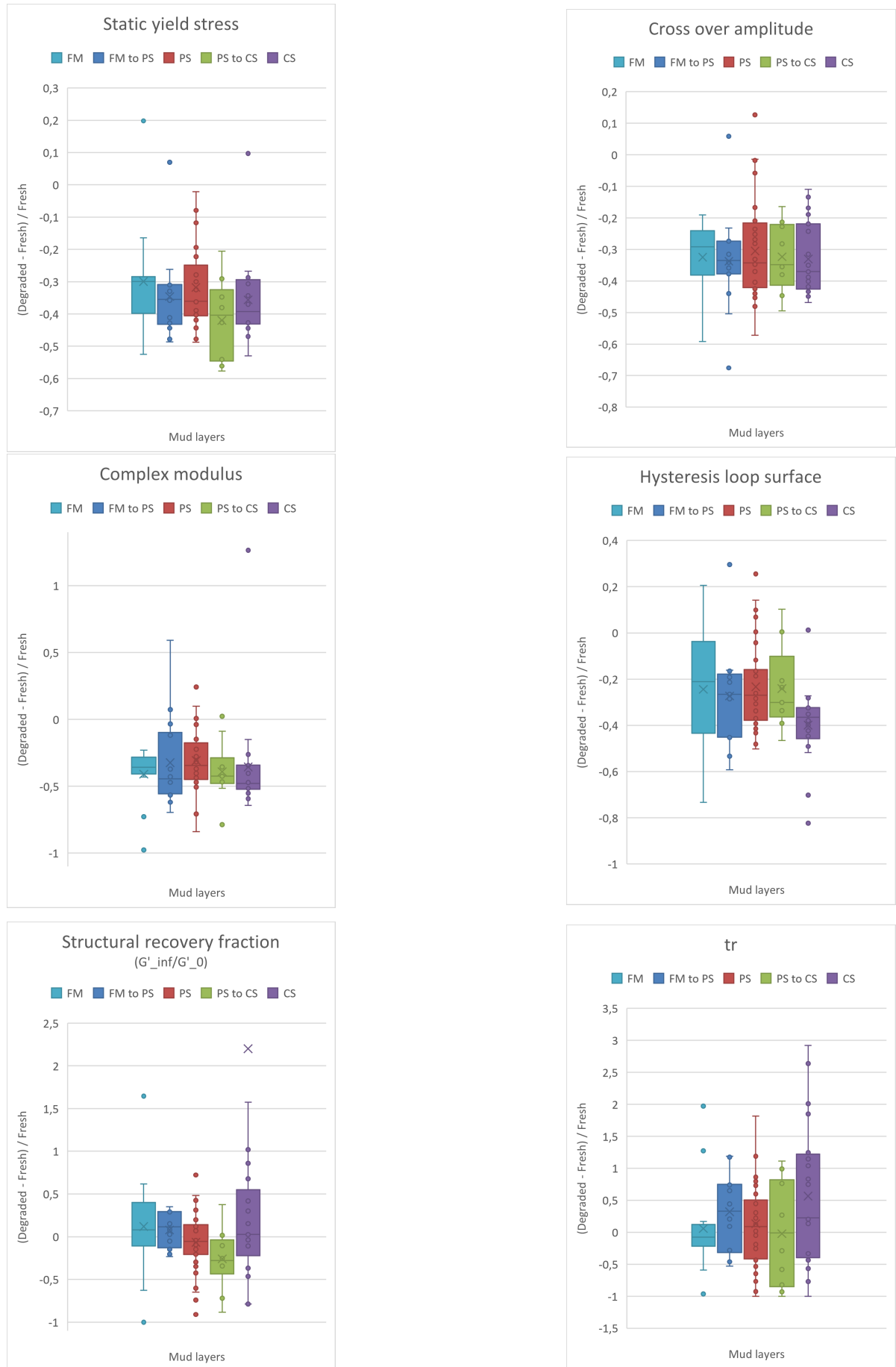
Figure E.3: Box plots of the relative differences of all τ_y^s, cross-over amplitudes, G^*, hysteresis loop surfaces, G_∞'/G_0' and tr for all locations, grouped by mud layer.
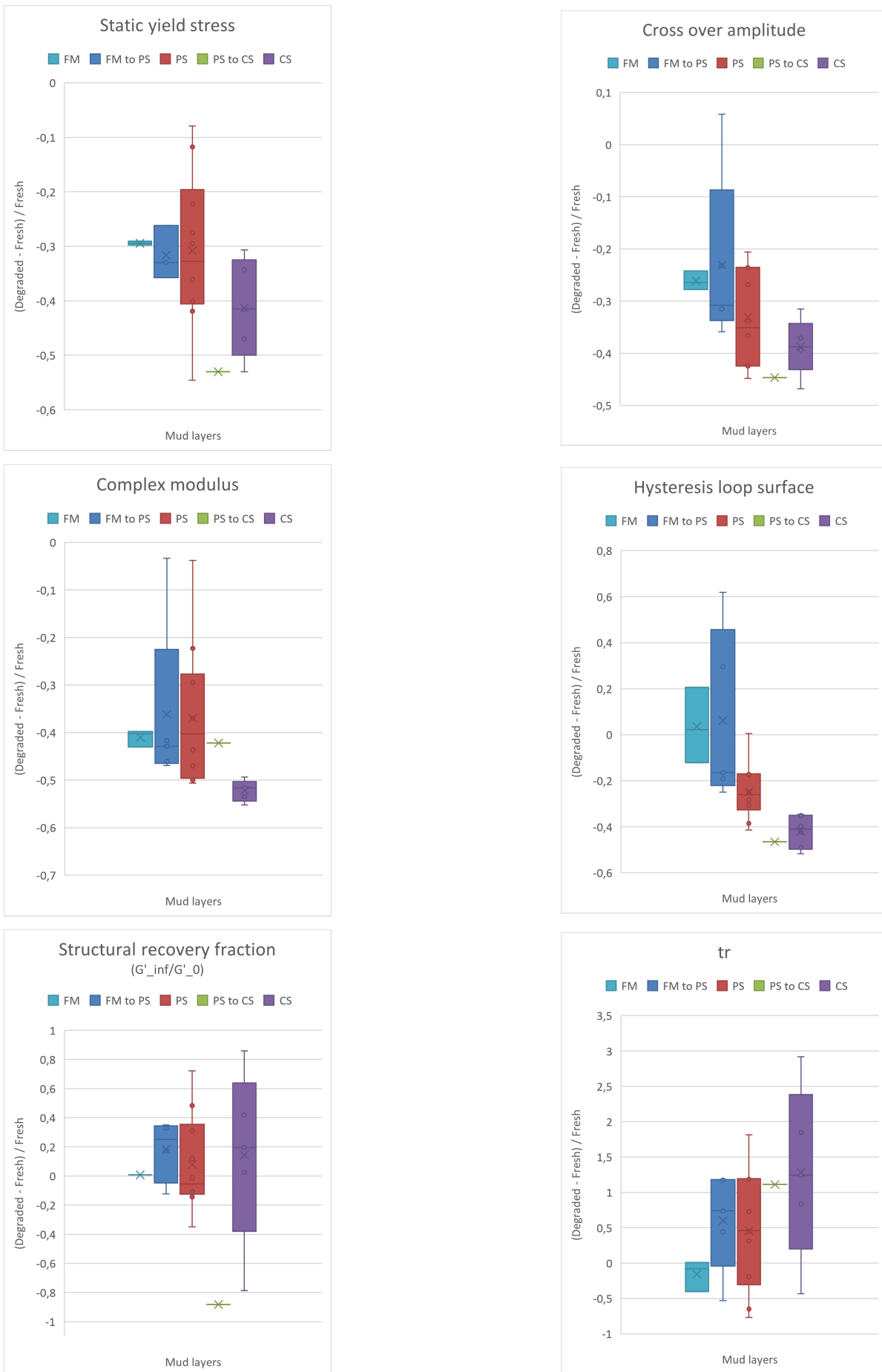
Figure E.4: Box plots of the relative differences of τ_y^s, cross-over amplitudes, G^*, hysteresis loop surfaces, G_∞'/G_0' and tr for location RT, grouped by mud layer.
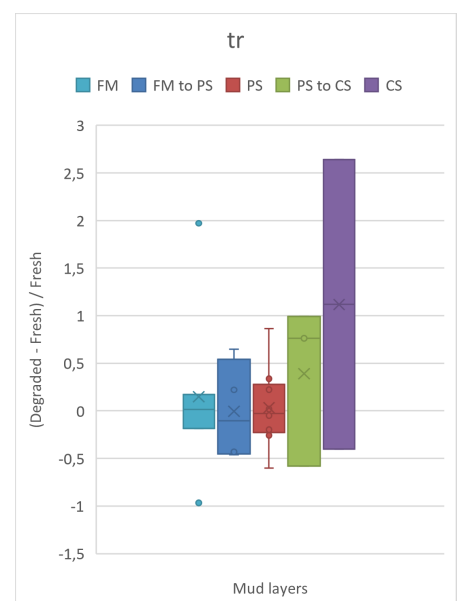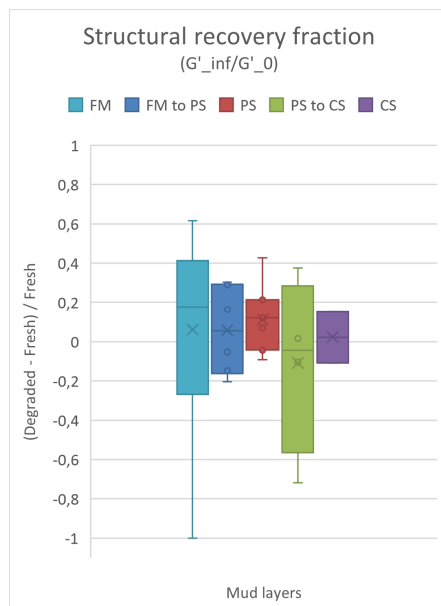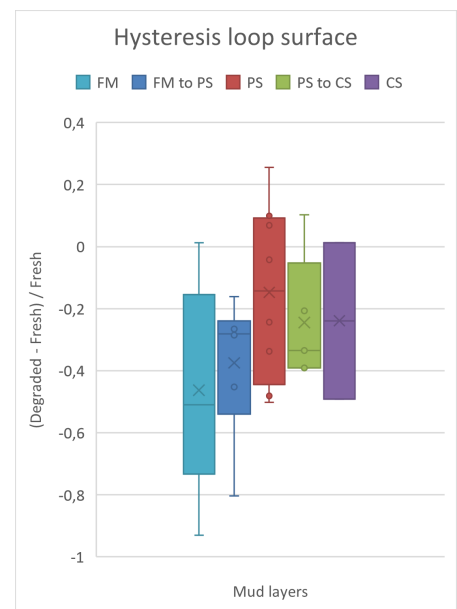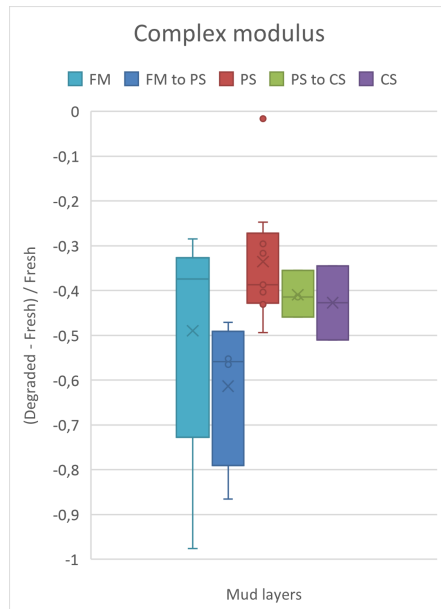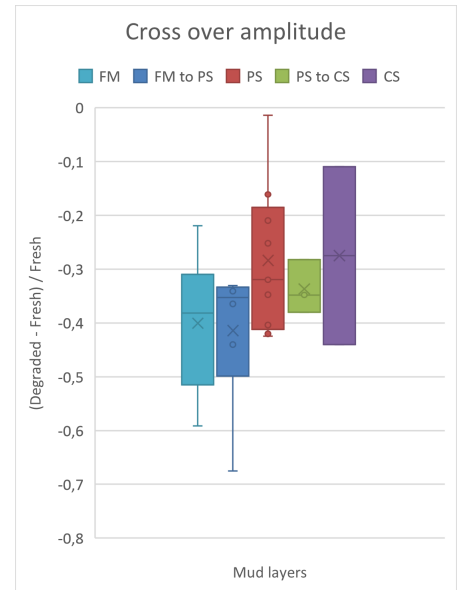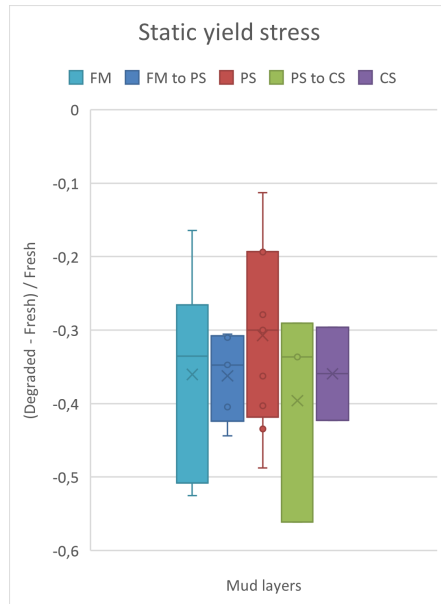
Figure E.5: Box plots of the relative differences of τ_y^s, cross-over amplitudes, G^*, hysteresis loop surfaces, $G_\infty{}'/G_0{}'$ and tr for location KH, grouped by mud layer.
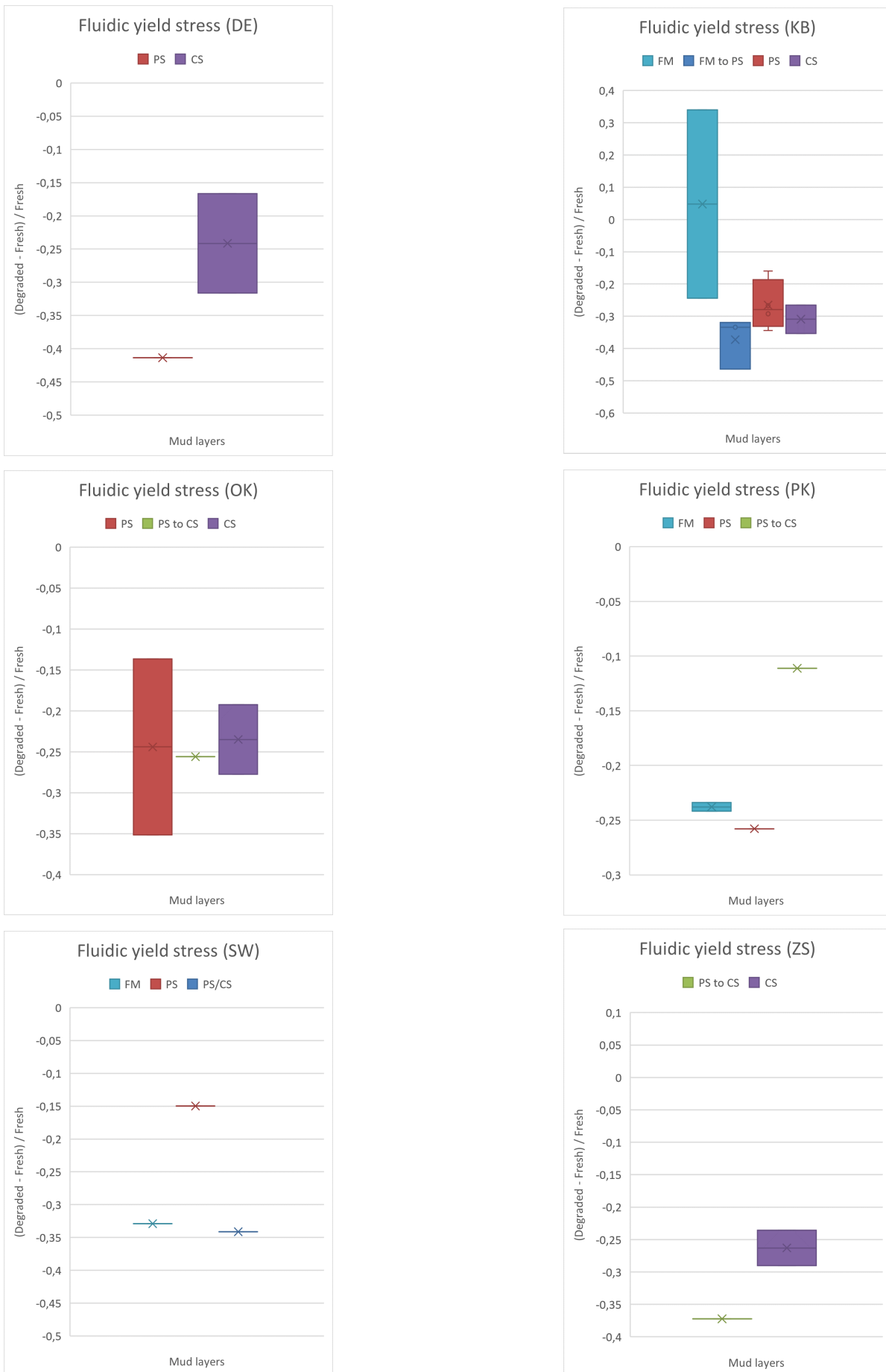
Figure E.6: Box plots of the relative differences of τ_y^f for locations DE, KB, OK, PK, SW and ZS, grouped by mud layer.
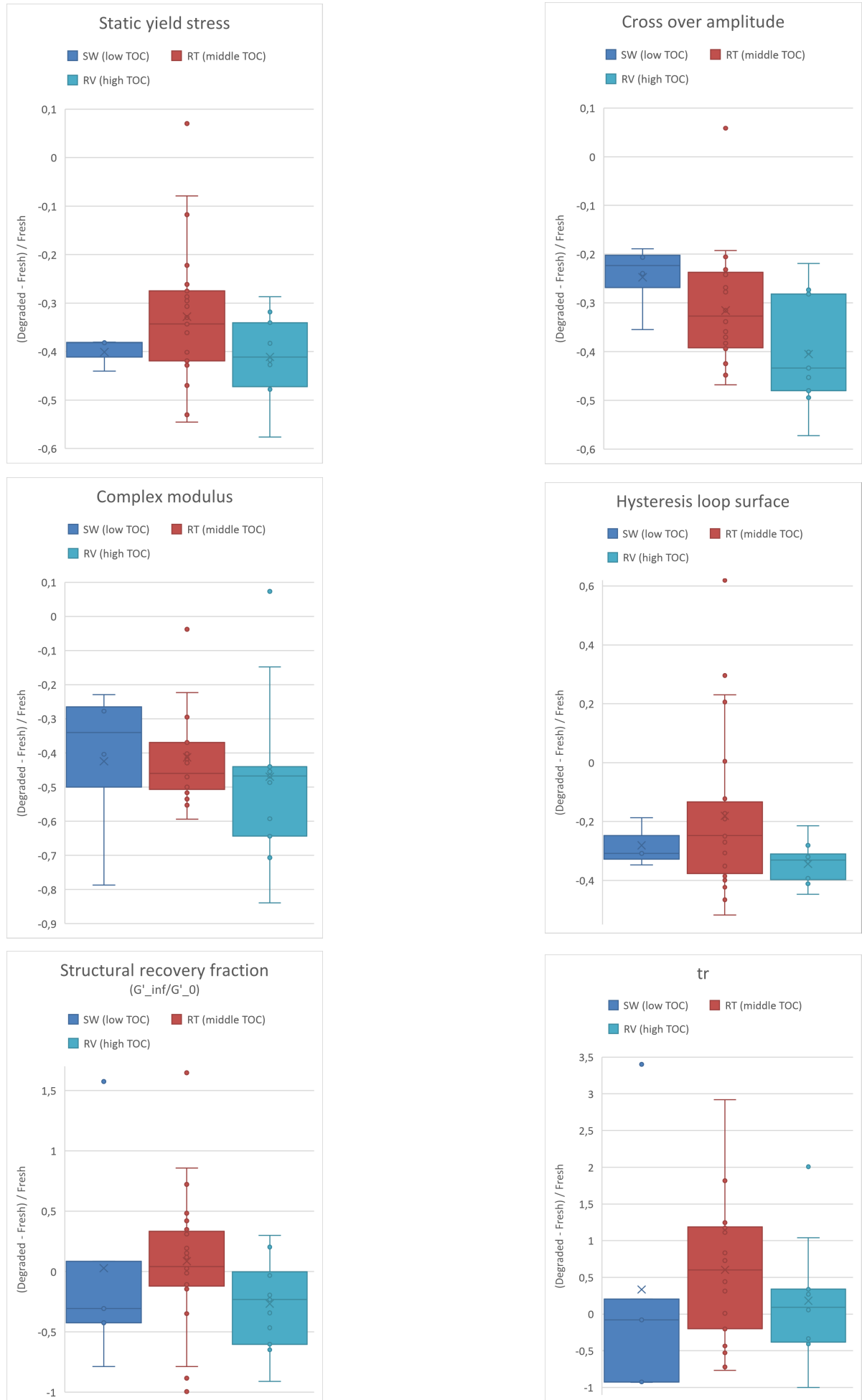
Figure E.7: Box plots of the relative differences of τ_y^s, cross-over amplitudes, G^*, hysteresis loop surfaces, $G_\infty{'}/G_0{'}$ and tr for the locations SW, RV and RT.
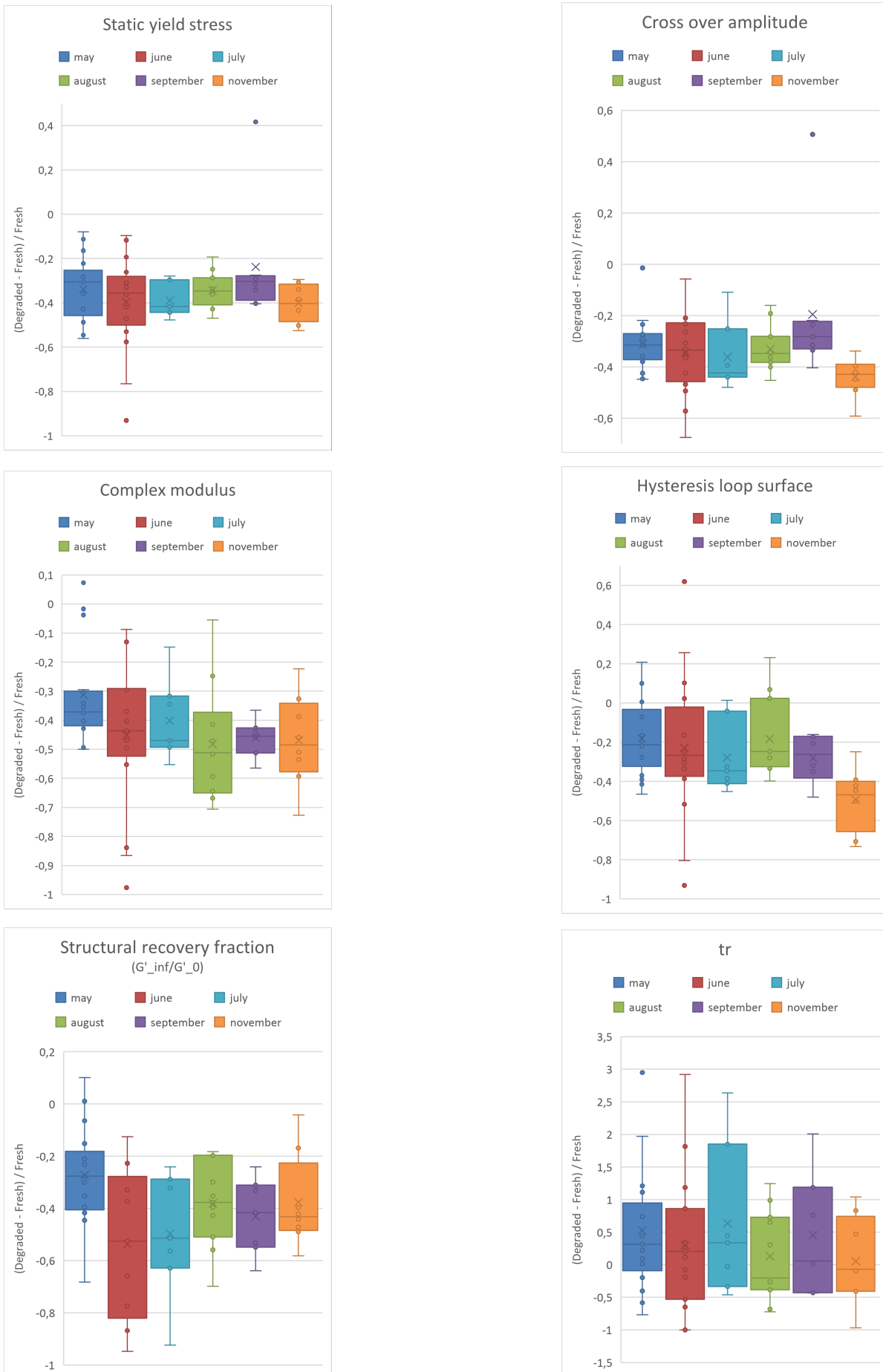
Figure E.8: Box plots of the relative differences of τ_y^s, cross-over amplitudes, G^*, hysteresis loop surfaces, G_∞'/G_0' and tr for the locations KH, RV and RT, sorted by sample month.
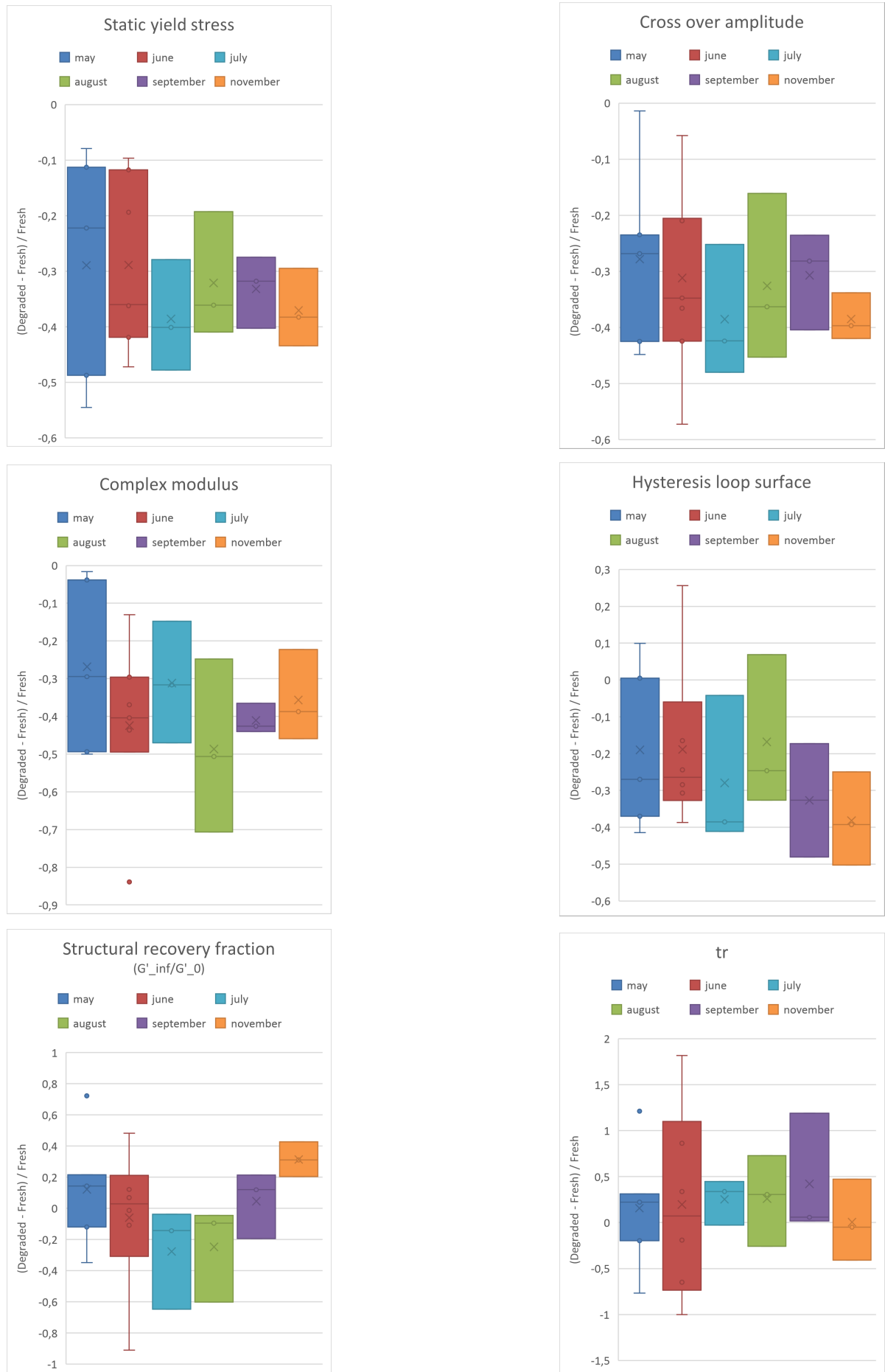
Figure E.9: Box plots of the relative differences of τ_y^s, cross-over amplitudes, G^*, hysteresis loop surfaces, $G_\infty{}'/G_0{}'$ and tr for the PS layers of the locations KH, RV and RT, sorted by sample month.

FM layer size

	6-5-2019	5-6-2019	3-7-2019	14-8-2019	24-9-2019	24-9-2019	5-11-2019	12-5-2020	27-5-2020	9-6-2020	22-6-2020	11-8-2020
■ layer size	40	30	30	40	10	10	10	60	80	160	60	40
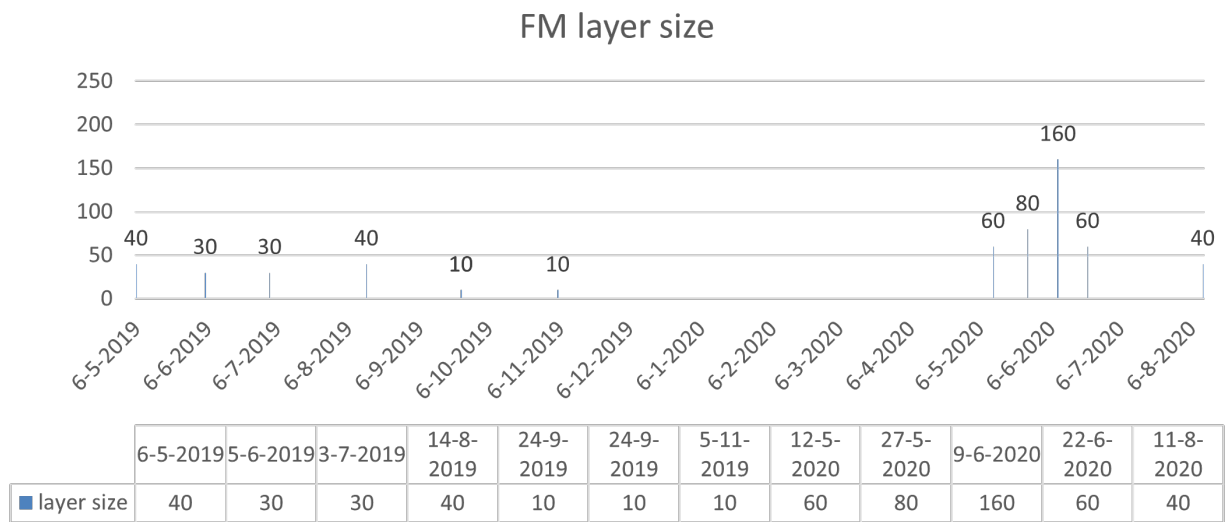
Figure E.10: The FM layer sizes of samples taken from location KH as a function of the sample dates.
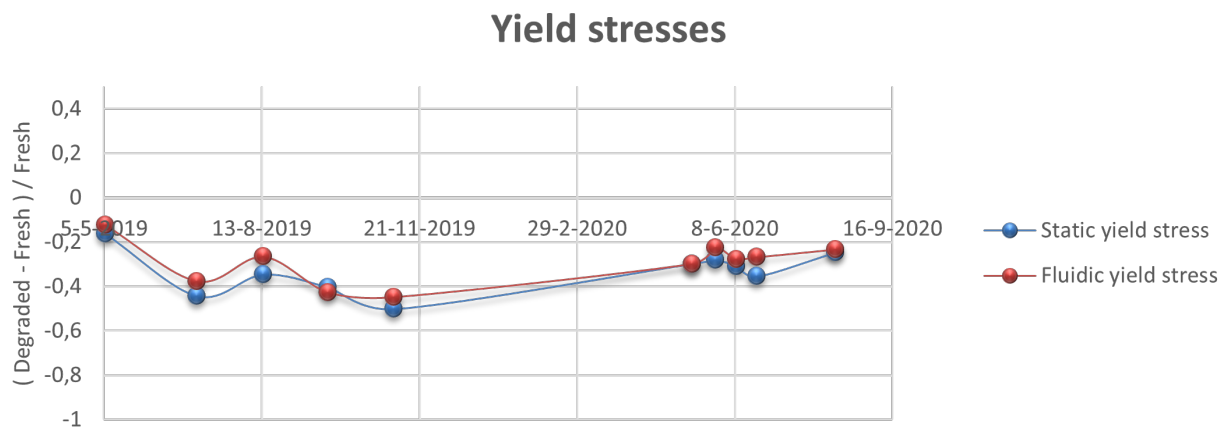
Yield stresses

Figure E.11: The FM yield stresses of samples taken from location KH as a funtion of the sample dates.
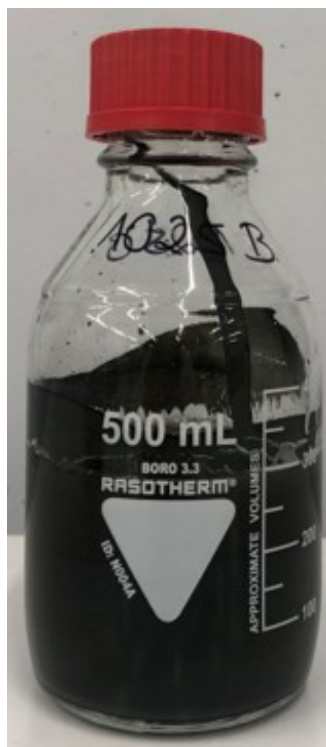
(a)
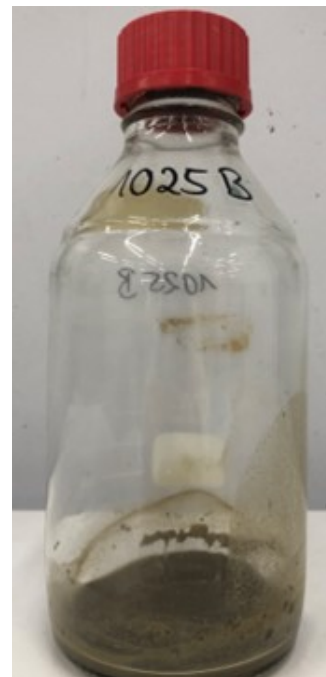
(b)

Figure E.12: Two pictures of degraded mud. Anaerobically on the left, an aerobically on the right. The pictures were taken by L. Alconcel.

Bibliography

Ahuja, A., Potanin, A., & Joshi, Y. M. (2020). Two step yielding in soft materials. *Advances in Colloid and Interface Science*, *282*, 102179. https://doi.org/10.1016/J.CIS.2020.102179

Arndt, S., Brumsack, H., & Wirtz, K. (2006). Cretaceous black shales as active bioreactors: A biogeochemical model for the deep biosphere encountered during odp leg 207 (demerara rise). *Geochimica et Cosmochimica Acta*, *70*, 408–425. https://doi.org/10.1016/j.gca.2005.09.010

Arndt, S., Jørgensen, B. B., LaRowe, D. E., Middelburg, J. J., Pancost, R. D., & Regnier, P. (2013). Quantifying the degradation of organic matter in marine sediments: A review and synthesis. *Earth-Science Reviews*, *123*, 53–86. https://doi.org/10.1016/J.EARSCIREV.2013.02.008

Bianchini, A., Cento, F., Guzzini, A., Pellegrini, M., & Saccani, C. (2019). Sediment management in coastal infrastructures: Techno-economic and environmental impact assessment of alternative technologies to dredging. *Journal of Environmental Management*, *248*, 109332. https://doi.org/https://doi.org/10.1016/j.jenvman.2019.109332

Boehlich, M. J., & Strotmann, T. (2008). Arch res technol north sea baltic coast 74. *Die küste* (pp. 288–306). Springer. https://izw.baw.de/publikationen/die-kueste/0/k074_ICCE_2008.pdf

Canfield, D., Kristensen, E., & Thamdrup, B. (2005). Aquatic geomicrobiology.

Coussot, P. (2017). *Mudflow rheology and dynamics*. https://doi.org/10.1201/9780203746349

De Leeuw, J. W., & Largeau, C. (1993). A review of macromolecular organic compounds that comprise living organisms and their role in kerogen, coal, and petroleum formation. In M. H. Engel & S. A. Macko (Eds.), *Organic geochemistry: Principles and applications* (pp. 23–72). Springer US. https://doi.org/10.1007/978-1-4615-2890-6_2

Devol, A. H. (1998). 35351. *391*(February), 2–4.

Gebert, J., Knoblauch, C., & Gröngröft, A. (2019). Gas production from dredged sediment. *Waste Management*, *85*, 82–89. https://doi.org/10.1016/j.wasman.2018.12.009

Gebert, J., Köthe, H., & Gröngröft, A. (2006). Prognosis of Methane Formation by River Sediments. *JSS-J Soils Sediments*, *6*(2), 75–83. https://doi.org/10.1065/jss2006.04.153

Grasset, C., Mendonça, R., Saucedo, G. V., Bastviken, D., Roland, F., & Sobek, S. (2018). Large but variable methane production in anoxic freshwater sediment upon addition of allochthonous and autochthonous organic matter. https://doi.org/10.1002/lno.10786

Haake mars rheometer instruction manual. (2014). https://www.researchgate.net/profile/Paulo_Matos4/post/How_to_covert_torque_vs_rpm_data_to_shear_stress_vs_shear_rate/attachment/5df0e8313843b0938395a2fd/AS%5C%3A834345451417601%5C%401575934865235/download/MARSI_III+Manual.pdf

Hedges, J., & Oades, J. (1997). Comparative organic geochemistries of soils and marine sediments. *Organic Geochemistry*, *27*(7), 319–361. https://doi.org/https://doi.org/10.1016/S0146-6380(97)00056-9

Jørgensen, B., & Sørensen, J. (1985). Seasonal cycles of o2, no3- and so42- reduction in estuarine sediments: The significance of an no3- reduction maximum in spring. *Marine Ecology-progress Series - MAR ECOL-PROGR SER*, *24*, 65–74. https://doi.org/10.3354/meps024065

Kirby, R., Parker, W. R., & van Oostrum, W. H. A. (2015). Definition of the seabed in navigation routes through mud areas. *The International Hydrographic Review*, *57*(1). https://journals.lib.unb.ca/index.php/ihr/article/view/23626

Kirby, R. (2010). Minimising harbour siltation: The economic and environmental future of ports. *Ports 2010: Building on the Past, Respecting the Future - Proceedings of the 12th Triannual International Conference*, 709–718. https://doi.org/10.1061/41098(368)73

Kirichek, A., Rutgers, R., Wensween, M., & van Hassent, A. (2018). Sediment management in the Port of Rotterdam. *2*(June 2018), 8.

Leys, V., & Mulligan, R. (2011). Modelling coastal sediment transport for harbour planning: Selected case studies. https://doi.org/10.5772/15007

McAnally, W. H., Friedrichs, C., Hamilton, D., Hayter, E., Shrestha, P., Rodriguez, H., Sheremet, A., & Teeter, A. (2007a). Management of Fluid Mud in Estuaries, Bays, and Lakes. I: Present State of Understanding on Character and Behavior. *Journal of Hydraulic Engineering*, *133*(1), 9–22. https://doi.org/10.1061/(asce)0733-9429(2007)133:1(9)

McAnally, W. H., Friedrichs, C., Hamilton, D., Hayter, E., Shrestha, P., Rodriguez, H., Sheremet, A., & Teeter, A. (2007b). Management of Fluid Mud in Estuaries, Bays, and Lakes. II: Present State of Understanding on Character and Behavior. *Journal of Hydraulic Engineering*, *133*(1), 9–22. https://doi.org/10.1061/(asce)0733-9429(2007)133:1(9)

Mewis, J., & de Bleyser, R. (1972). Dynamic behavior of thixotropic systems. *Journal of Colloid and Interface Science*, *40*(3), 360–369. https://doi.org/https://doi.org/10.1016/0021-9797(72) 90345-1

Mobuchon, C., Carreau, P. J., & Heuzey, M.-C. (2007). Effect of flow history on the structure of a non-polar polymer/clay nanocomposite model system. *Rheologica Acta*, *46*, 1045–1056.

Mobuchon, C., Carreau, P. J., & Heuzey, M.-C. (2009). Structural analysis of non-aqueous layered silicate suspensions subjected to shear flow. *Journal of Rheology*, *53*(5), 1025–1048. https://doi.org/10.1122/1.3193720

Morrison, F., & Morrison, A. (2001). *Understanding rheology*. Oxford University Press. https://books.google.nl/books?id=bwTn8ZbR0C4C

Nie, S., Jiang, Q., Cui, L., & Zhang, C. (2020). Investigation on solid-liquid transition of soft mud under steady and oscillatory shear loads. *Sedimentary Geology*, *397*, 105570. https://doi.org/https://doi.org/10.1016/j.sedgeo.2019.105570

OSPAR. (2016). OSPAR annual report on dumping and placement of wastes or other matter at sea in 2014. ISBN: 978-1-911458-01-2. Publication number: 671/2016.

Parker, W. R., & Kirby, R. (1982). Time dependent properties of cohesive sediment relevant to sedimentation management-european experience.

Pellegrini, M., Preda, G., & Saccani, C. (2020). Application of an innovative jet pump system for the sediment management in a port channel: Techno-economic assessment based on experimental measurements. *Journal of Marine Science and Engineering*, *8*(9). https://doi.org/10.3390/jmse8090686

PIANC. (2014). Harbour approach channels design guidelines.

Pūtaiao, S. L. H. P. A. (2010). Non-newtonian fluids. https://www.sciencelearn.org.nz/resources/1502-non-newtonian-fluids

Rehitha, T., Ullas, N., Vineetha, G., Benny, P., Madhu, N., & Revichandran, C. (2017). Impact of maintenance dredging on macrobenthic community structure of a tropical estuary. *Ocean Coastal Management*, *144*, 71–82. https://doi.org/https://doi.org/10.1016/j.ocecoaman.2017.04.020

Robador A, J. B., Brüchert V. (2009). The impact of temperature change on the activity and community composition of sulfate-reducing bacteria in arctic versus temperate marine sediments. *Measurement: Journal of the International Measurement Confederation*.

Scböl, A., Hein, B., Wyrwa, J., & Kirchesch, V. (2014). Modelling water quality in the elbe and its estuary -large scale and long term applications with focus on the oxygen budget of the estuary. *Kuste*, 203–232.

Shakeel, A., A., K., A., T., & C., C. (2021). Rheological analysis and rheological modelling of mud sediments: What is the best protocol for maintenance of ports and waterways? *Estuarine, Coastal and Shelf Science*, *257*, 107407. https://doi.org/https://doi.org/10.1016/j.ecss.2021.107407

Shakeel, A., Kirichek, A., & Chassagne, C. (2019). Is density enough to predict the rheology of natural sediments? *Geo-Marine Letters*, *39*(5), 427–434. https://doi.org/10.1007/s00367-019-00601-2

Shakeel, A., Kirichek, A., & Chassagne, C. (2020a). Effect of pre-shearing on the steady and dynamic rheological properties of mud sediments. *Marine and Petroleum Geology*, *116*(March), 104338. https://doi.org/10.1016/j.marpetgeo.2020.104338

Shakeel, A., Kirichek, A., & Chassagne, C. (2020b). Effect of pre-shearing on the steady and dynamic rheological properties of mud sediments. *Marine and Petroleum Geology*, *116*, 104338. https://doi.org/https://doi.org/10.1016/j.marpetgeo.2020.104338

Shakeel, A., Kirichek, A., & Chassagne, C. (2020c). Rheological analysis of mud from Port of Hamburg, Germany. *Journal of Soils and Sediments*, *20*(6), 2553–2562. https://doi.org/10.1007/s11368-019-02448-7

Shakeel, A., Kirichek, A., & Chassagne, C. (2020d). Rheological analysis of natural and diluted mud suspensions. *Journal of Non-Newtonian Fluid Mechanics*, *286*(May), 104434. https://doi.org/10.1016/j.jnnfm.2020.104434

Shakeel, A., Kirichek, A., & Chassagne, C. (2020e). Yield stress measurements of mud sediments using different rheological methods and geometries: An evidence of two-step yielding. *Marine Geology*, *427*(May), 106247. https://doi.org/10.1016/j.margeo.2020.106247

Shakeel, A., Kirichek, A., & Chassagne, C. (2020f). Yield stress measurements of mud sediments using different rheological methods and geometries: An evidence of two-step yielding. *Marine Geology*, *427*(May), 106247. https://doi.org/10.1016/j.margeo.2020.106247

Shakeel, A., MacIver, M. R., van Kan, P. J., Kirichek, A., & Chassagne, C. (2021). A rheological and microstructural study of two-step yielding in mud samples from a port area. *Colloids and Surfaces A: Physicochemical and Engineering Aspects*, *624*, 126827. https://doi.org/10.1016/J.COLSURFA.2021.126827

Shakeel, A., van Kan, P. J., & Chassagne, C. (2019). Design of a parallel plate shearing device for visualization of concentrated suspensions. *Measurement: Journal of the International Measurement Confederation*, *145*, 391–399. https://doi.org/10.1016/j.measurement.2019.05.101

Sharp, J. A., Johnson, H., Pevey, K., & McAnally, W. (2010). Sediment management alternatives for the port of bienville.

Shenoy, A. V., & Saini, D. R. (n.d.). *Melt Flow Index: More Than Just A Quality Control Rheological Parameter. Part I* (tech. rep.).

Six, J., & Paustian, K. (2014). Aggregate-associated soil organic matter as an ecosystem property and a measurement tool. *Soil Biology and Biochemistry*, *68*, A4–A9. https://doi.org/10.1016/J.SOILBIO.2013.06.014

Varga, Z., Grenard, V., Pecorario, S., Taberlet, N., Dolique, V., Manneville, S., Divoux, T., McKinley, G. H., & Swan, J. W. (2019). Hydrodynamics control shear-induced pattern formation in attractive suspensions. *Proceedings of the National Academy of Sciences of the United States of America*, *116*(25), 12193–12198. https://doi.org/10.1073/pnas.1901370116

Yao, H., Conrad 1'*, R., Wassmann, R., & Neue, H. U. (1999). *Effect of soil characteristics on sequential reduction and methane production in sixteen rice paddy soils from China, the Philippines, and Italy* (tech. rep. No. 9). KluwerAcademic Publishers.

Zander, F., Shakeel, A., Kirichek, A., Chassagne, C., & Gebert, J. (2022). Effects of organic magger degradation in cohesive sediment: Linking sediment rheology to spatio-temporal patterns of organic matter degradability. *Journal of soils and sediments (under review)*.

Zander, F., Heimovaara, T., & Gebert, J. (2020). Spatial variability of organic matter degradability in tidal Elbe sediments. *Journal of Soils and Sediments*, *20*(6), 2573–2587. https://doi.org/10.1007/s11368-020-02569-4